

THE MYSTERY OF THE WHELK EGG CAPSULE PROTEIN -
ELECTROSPINNING, MECHANICAL TESTING, AND BEING OUTSMARTED BY
AN INVERTEBRATE

by

CARLA M. CORBETT

BSc., The University of British Columbia, 2006

A THESIS SUBMITTED IN PARTIAL FULFILLMENT OF
THE REQUIREMENTS FOR THE DEGREE OF
MASTER OF SCIENCE

in

THE FACULTY OF GRADUATE STUDIES

(Zoology)

THE UNIVERSITY OF BRITISH COLUMBIA

(Vancouver)

August 2010

© Carla M. Corbett, 2010

ABSTRACT

Whelks are carnivorous marine snails known for their elaborate and durable egg capsules. The mechanically complex capsules have been previously studied, and shown to have mechanical behaviour similar to keratin. The mature protein has an initial stiff linear elastic region at low strain, followed by a rubbery yield region with a fully repeatable order of magnitude decrease in stiffness. The material properties of the protein mature in distinct stages, with long-range elasticity developing first, followed by the development of the stiff Hookean region. As the capsule matures, it is massaged by a gland in the foot of the snail, which probably enables cross-linking.

This study sought to mimic the development process using electrospinning to create fibres with charge-based assembly, then adding a cross-linking step to encourage the stiff spring behaviour to form. An electrospinning protocol was developed and parameters were optimized. The technique was applied successfully, and the resulting protein nanofibres could be cross-linked. The electrospun protein fibres were shown to have composition and secondary structures similar to the native protein. However, the mechanical properties of the cross-linked nanofibres were more similar to a transitional stage in the egg capsule's maturation sequence than they were to the mature capsule. The fibres did not exhibit the bimodal behaviour seen in the native polymer.

TABLE OF CONTENTS

Abstract	ii
Table of Contents	iii
List of Tables	vi
List of Figures	vii
Acknowledgements	ix
Dedication	x
1 Introduction	1
1.1 The goal	1
1.2 Background	1
1.3 Egg capsule formation	3
1.4 Structure of the capsule	4
1.5 Structure of the protein	6
1.6 Mechanical properties	7
1.7 Maturation model	9
1.8 More mechanical properties	12
1.9 Polarized light microscopy	13
1.10 FTIR	14
1.11 Biomimetics and electrospinning	15
1.12 History of electrospinning	16
1.13 Electrospinning technique	18
1.14 Electrospinning parameters	19
1.15 Hypothesis	21

2	Methods	22
2.1	Preparation of solutions	22
2.2	Selection of TCEP	22
2.3	Nanofibre electrospinning	23
2.4	Preparation of SEM samples	25
2.5	Collection of SEM images	25
2.6	Polarized light microscopy	26
2.7	Effect of PEO	27
2.8	Measurement of fibres	27
2.9	FTIR spectroscopy	28
2.10	Preparation of samples for testing	29
2.11	Testing apparatus	31
2.12	Testing procedure	33
3	Results	36
3.1	Effect of TCEP	36
3.2	Effect of parameters	37
3.3	Polarized light microscopy	39
3.4	Effect of PEO	40
3.5	Measurement of fibres	42
3.6	FTIR spectra	45
3.7	Results of mechanical testing	47

4	Discussion	50
4.1	Electrospinning parameters	50
4.2	PEO	54
4.3	Nanofibre diameter	55
4.4	Birefringence of fibres	56
4.5	Matrix Squeeze	57
4.6	Self assembly	58
4.7	FTIR to identify	59
4.8	FTIR to determine structure	60
4.9	Cross-linking	62
4.10	Mechanical testing	63
4.11	Mechanical results	64
4.12	Future directions	66
	References	68

LIST OF TABLES

Table 1	Blend solution concentration series	28
Table 2	Characteristic amide I band frequencies	29
Table 3	Composition of protein and electrospun fibres	45
Table 4	Young's modulus and hysteresis	49
Table 5	Secondary structure of common structural proteins	61

LIST OF FIGURES

Figure 1	Whelk morphology	2
Figure 2	Production of egg capsules	3
Figure 3	Stress/strain curve for 15 extension cycles	7
Figure 4	Capsule maturation timeline	8
Figure 5	Model of WECB mechanics through maturation	10
Figure 6	Reversible α -helix to β -sheet transition during straining	11
Figure 7	Stress recovery	12
Figure 8	Electrospinning technique diagram	19
Figure 9	The Kato Tech NEU-010	24
Figure 10	Diagram of modified electrospinning technique	30
Figure 11	Electrospun fibres span the gap	31
Figure 12	Microscope-based micro-tensile testing apparatus	32
Figure 13	Samples were glued to a glass micro-beam	34
Figure 14	Diagram of SDS-PAGE gel	37
Figure 15	Effect of electrospinning parameters	38
Figure 16	Birefringence of electrospun fibres	39
Figure 17	Electrospun PEO fibres at different concentrations	41
Figure 18	Results of washing electrospun fibres	42
Figure 19	Mean diameters of electrospun fibres	42
Figure 20	Mean diameters of PEO fibres	43
Figure 21	Mean diameters of analogous solutions	44
Figure 22	Mean diameters of fibres before and after washing	44

Figure 23	FTIR spectra	46
Figure 24	Stress-strain curves	48
Figure 25	Hysteresis loops	48

ACKNOWLEDGEMENTS

It's over!

I have so many people to thank for so much.

First of all, thanks to Bob, the world's best supervisor, for the incredible patience, the amazing support, and the awesome sense of humour.

Thanks to John, my grand-supervisor, for getting me into this in the first place. Wait, should I be thanking you for that?

Thanks to my dad, who took over my tractor payments so I could actually finish my thesis without having to declare bankruptcy. I promise I'll pay you back.

Thanks to my mom, for the endless baking – it's all about healthy nutrition.

Thanks to all my family and friends for their help on the farm, you guys made it possible for me to get to the lab.

A humble thank you for the endless love, support, affection, and patience from my sweet Habib, who has been sorely neglected during the course of my graduate work. That poor horse sat through more practice runs of my defense presentation than any human would ever have done.

Finally, thanks to Cam for not only putting up with me, but deciding to marry me while I went through all the lovely stress of pulling this together. You must be nuts, honey.

C

For Gramps

1 Introduction

1.1 *The goal*

The aim of this study was to try to solve a mystery. A very cool self-assembling biomaterial goes through a poorly understood maturation process during which interesting mechanical properties develop. We believe that the process involves charge-based assembly and a cross-linking step. In order to understand the maturation process, we worked to recreate the polymer from its precursor, using the electrospinning technique. Electrospinning a solution of the immature material induces the formation of nano-scale fibres, which are aligned and assembled by charge. Adding a cross-linking agent to the electrospun nanofibres should alter the mechanical properties of the fibres and take them one step further in the maturation process. Ideally, we will come close to the properties of the native material, and this will help elucidate the maturation process. If we can mimic the process and produce the material in manageable form, we can harness its mechanical properties for industrial or medical applications.

1.2 *Some background on whelks and egg capsules*

Whelks are a species-rich group of marine Prosobranch snails found in temperate waters. Whelks are fascinating not only because they are voracious carnivores with a deceptively benign appearance, or because of their alternative lifestyle (they are serial hermaphrodites who first develop sexually as males, then mature and realize their full potential as females), or because an enormous whelk is the first evil boss encountered in the video game Final Fantasy VI, but also for their creative industry in producing “mermaids’ necklaces”, as their strings of egg cases are sometimes called.

Whelks are known for these strings of pale, disk-shaped egg capsules, commonly found on beaches along the east coast of Canada and the United States. The egg cases are

highly resilient and are composed primarily of an insoluble protein polymer (whelk egg capsule protein, WECP). The polymer shares properties with other major structural proteins: it has hierarchical ordering like collagen, long-range elasticity like elastin, and mechanical behaviour like keratin.



Figure 1. Whelk morphology. Whelks are carnivorous marine snails found all over the world in a variety of shapes and sizes. Females deposit developing embryos in highly resilient proteinaceous egg cases that show species-specific morphology.

The egg capsules are physically and chemically stable, and are able to withstand the harsh marine environment for months over winter while the embryos develop. In fact, when the embryos come full term, looking like scaled-down versions of adult whelks, the juveniles escape from the egg capsule by means of a mucosal plug, leaving the capsule itself unharmed.

The capsules have fascinating mechanical properties. They are reversibly elastic and can be repeatedly stretched to high extensions without apparent damage. At small extensions, the material acts like a stiff spring, with most of the elastic strain energy recovered by recoil. However, at larger extensions the material yields and becomes rubbery, with much lower resilience and elastic stiffness. These dramatic changes are quickly and completely reversible for extensions of 80% in repeated loading cycles. Shockingly, the stiff spring behaviour can even rapidly reform in the rubbery region if the extension is interrupted and the strain held constant.

Many adaptive functions have been suggested for these energetically expensive egg capsules, including protection against desiccation, predation, UV irradiation, osmotic stresses, and the impact loading encountered in the intertidal zone (Ojeda and Chaparro, 2004; Pechenik, 1979). However, none of these potential roles has yet been blessed with strong experimental support, so the protective role of the capsules remains controversial.

1.3 Egg capsule formation

A precursor protein of WECB is found in the nidamental gland, where capsule formation is initiated. Embryos are wrapped in a soft, pliable sack by nidamental gland mesodermal secretory cells before leaving the genital tract. This preliminary capsule is passed out of the body and under a depression in the foot called the ventral pedal gland (VPG). Here the capsule is massaged and manipulated by the muscle surrounding the gland for about an hour before it is deposited on the substratum. The capsules may be deposited individually, or joined to a growing strand that is then attached to the substratum as a unit.

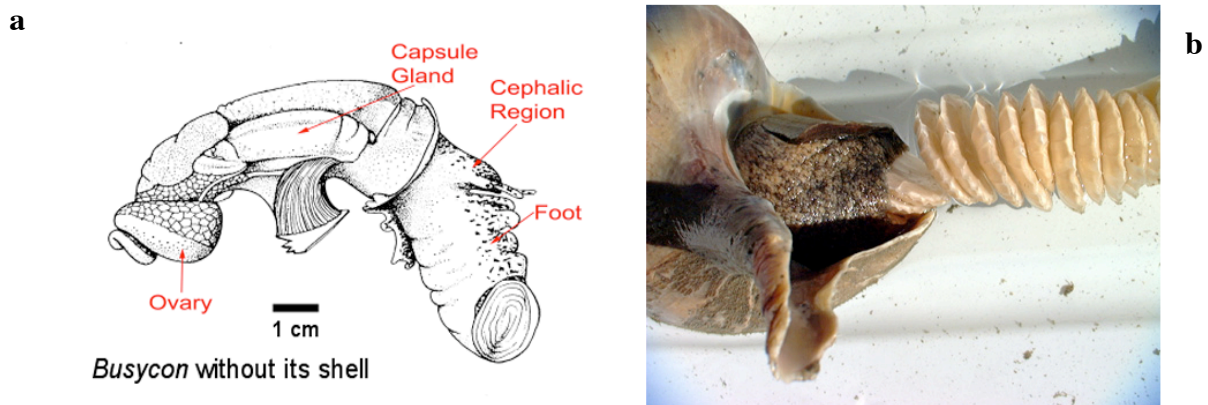


Figure 2. Production of egg capsules. (a) Embryos travel from the ovary down the reproductive tract to the nidamental gland, where they are wrapped in a soft sack – the immature egg capsule. Egg capsules are formed from protein synthesized and stored in the nidamental gland. (b) Embryos are packaged into immature capsules, which pass out of the body and into a depression in the foot called the ventral pedal gland, where they are processed before deposition on the substratum.

During the manipulation period some unknown physical and/or chemical process renders the capsule relatively rigid and insoluble. Capsules removed from a whelk before treatment in the VPG are soluble and have no tensile integrity. This suggests that the VPG processing involves polymer stabilization via covalent crosslinking (Rapoport and Shadwick, 2007). Interestingly, egg capsule production can be induced in gravid females by injection with an extract of the circumesophageal ganglion, but the resulting capsules remain “unhardened”, much like the natural capsules without treatment by the VPG. These observations suggested that the immature capsule, the whelk egg capsule gland protein (WECGP), would be useful in future studies on the natural polymerization process.

1.4 Structure of whelk egg capsules

In an early study, Hunt (1966) reported that the egg capsule of the whelk *Buccinum undatum* was composed of 77.5% amino acids and 5-6% sugars. At that time, the source of the egg capsule material was unknown. We now know that the egg capsules are extracellular constructs composed of over 80% protein – the rest is lipids and carbohydrates (Sullivan and Mangel, 1984).

Early descriptive work on whelk egg capsules found a large degree of species-specific morphological variation, which has since been attributed to morphological variation in the VPG itself. That is, differently shaped glands produce differently shaped capsules. It has also been demonstrated that within a species, snails of different size produce scaled versions of egg capsules of similar morphology.

Unlike a typical amorphous rubbery polymer, whelk egg capsules are highly birefringent, with a layered structure and a fibrous appearance. Light microscopy shows that the capsules are made of numerous distinct layers of material, and transmission electron microscopy (TEM) shows that the layers have striated patterns, similar to

collagen, keratin, and some chitins (Rapoport and Shadwick, 2002). Rapoport and Shadwick (2002) also found that the capsules are composed of fibres approximately 0.3 μm in diameter and that the laminae of the capsule walls have a characteristic banding pattern of 48 to 52 nm.

Early X-ray diffraction studies showed that the fibrils that form the striated pattern have an α -helical conformation (Flower et al., 1969). Rawlings (1999) showed that the capsules have hierarchical layers of ordered fibres. These observations suggest a structure analogous to an intermediate filament (IF)-based material such as hard α -keratin, but there are important differences in structure and formation (Rapoport and Shadwick, 2007).

WECB is composed of discrete plywood-like sheets of fibrous material arranged at different angles and exhibits isotropic mechanical behaviour in the plane formed by the transverse and longitudinal axes of the capsule (Rapoport and Shadwick, 2007). Hard α -keratin, on the other hand, is a complex cylindrically arranged composite with concentric hierarchical layers around a major axis of fibrillar orientation (Hearle, 2000). The precursor of WECB, WECGP, is an extracellular material stored in glandular vesicles, while hard α -keratin is derived from epithelial cells in a complex biogenic process, and contains cellular remnants (Van Steensel et al., 2000).

The egg capsules have their fibrous hierarchical arrangement at all stages of processing, even as mechanical integrity is developing (Rapoport and Shadwick, 2007). Scanning electron microscopy (SEM) comparisons show that the mechanical integrity does not arise from any gross structural changes resulting from the manipulations of the VPG – the capsule structure is completed in the nidamental gland, and VPG treatment somehow causes it to become an insoluble protein polymer (Rapoport and Shadwick, 2007). VPG activity likely induces the formation of cross-links and possibly adds matrix (Rapoport and Shadwick, 2007).

1.5 Structure of whelk egg capsule protein

Amino acid analysis shows that the WECP is rich in both acidic and basic amino acids (Hunt, 1966; see also Rapoport and Shadwick, 2002). Flower et al. (1969) proposed that a number of α -helices either aggregate into a large, complex unit, or form a multi-strand coiled-coil. Their X-ray diffraction and electron microscopy results suggested that the α -helical units do not have a precise repeat pattern, but have some degree of orientation about their long axis (Flower et al., 1969).

Flower (1973) stated that two protein structures, “ribbons” and “filaments”, are used by the whelks to produce egg capsules. The two protein structures were supposed to be produced and stored separately (Flower, 1973). However, Goldsmith et al. (1977) used digestions, amino acid composition studies, and electron microscopy to conclude that the soluble precursor protein (which they named “precapsulin”) was likely only one species of protein being cross-linked into dimers, trimers, and tetramers.

The egg capsules resist both enzymatic degradation and common protein solvents (such as formic acid, sodium dodecyl sulphate (SDS), and urea), which also suggests that the material contains cross-links. Cross-links likely give the material its mechanical properties as well. Hunt (1966) determined that the insolubility of the material should not be attributed to disulphide cross-links, because the capsule has a low concentration of sulphur-containing amino acids. Rapoport and Shadwick (2002) found that cysteine is also completely absent in *Busycon*, and is only present in trace amounts in other species. However, a very small number of disulphide cross-links may be sufficient to give the material its properties. Agents that selectively reduce disulphide bonds, such as dithiothreitol (DTT) and Tris [2-carboxyethyl] phosphine (TCEP), were effective in breaking WECCGP into its monomeric subunit.

1.6 Mechanical properties of whelk egg capsules

The mechanical properties of the capsules are intriguing. They are reversibly elastic and can be repeatedly stretched to high extensions (over 80%) without apparent damage. At small extensions (>3-5%), the material acts like a stiff spring, with most of the elastic strain energy recovered by recoil. This initial stiff portion of the stress-strain curve is called the “Hookean” region, due to its linear elastic response. The Hookean region is characterized by a relatively high modulus of elasticity and low hysteresis.

At larger extensions the capsule yields and becomes rubbery, with much lower resilience and elastic stiffness. This portion of the stress-strain curve is plateau-like, has a relatively low modulus and high hysteresis, and is called the “yield” region. The dramatic changes between the two regions are completely reversible, in a second or less, for extensions of 80% in repeated loading cycles. Remarkably, the stiff spring behaviour of the Hookean region quickly reforms in the yield region if the extension process is interrupted.

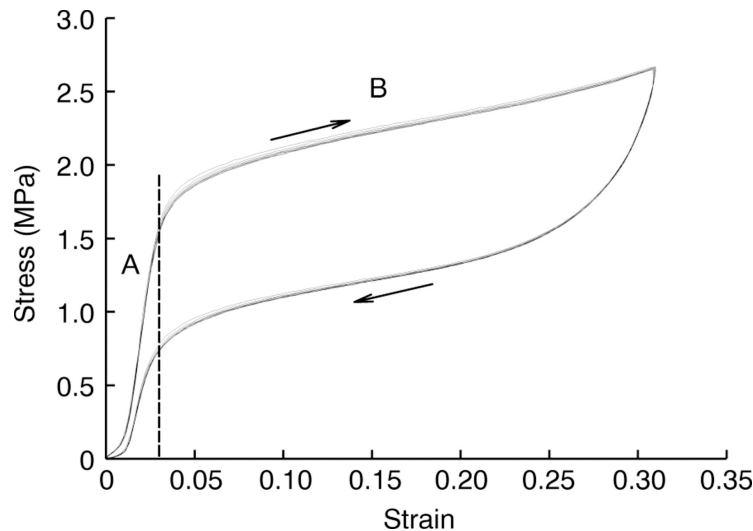


Figure 3. 15 extension cycles for a 6mm wide strip of mature egg capsule from *B. canaliculatum*. Region A is called the Hookean region due to its linear elastic behaviour, region B is the yield region. The dashed line at approximately 3% strain is the yield point, where the material undergoes a reversible, order of magnitude decrease of elastic modulus, from 87.9 MPa in A to 3.9 MPa in B. The arrows indicate the direction of the strain during the extension cycles. Reproduced with permission from Journal of Experimental Biology, Rapoport and Shadwick 2007.

Rapoport and Shadwick (2002) proposed that two hierarchical levels of stabilization exist in the material, one giving high stiffness seen at small extensions, the other giving the elasticity seen at high extensions. The first, high Young's modulus level of stabilization is labile to strain and high temperature, but is fully recoverable upon return to its native condition (Rapoport and Shadwick, 2002). The second, low modulus level is stable, and is likely to exist in the immature capsule prior to cross-linking (Rapoport and Shadwick, 2007). Qualitative observations suggest that the bimodal behaviour of WECP develops sequentially, with the simpler rubber-like behaviour of the yield region developing first, and the Hookean region developing later in the capsule maturation process (Rapoport and Shadwick, 2007).

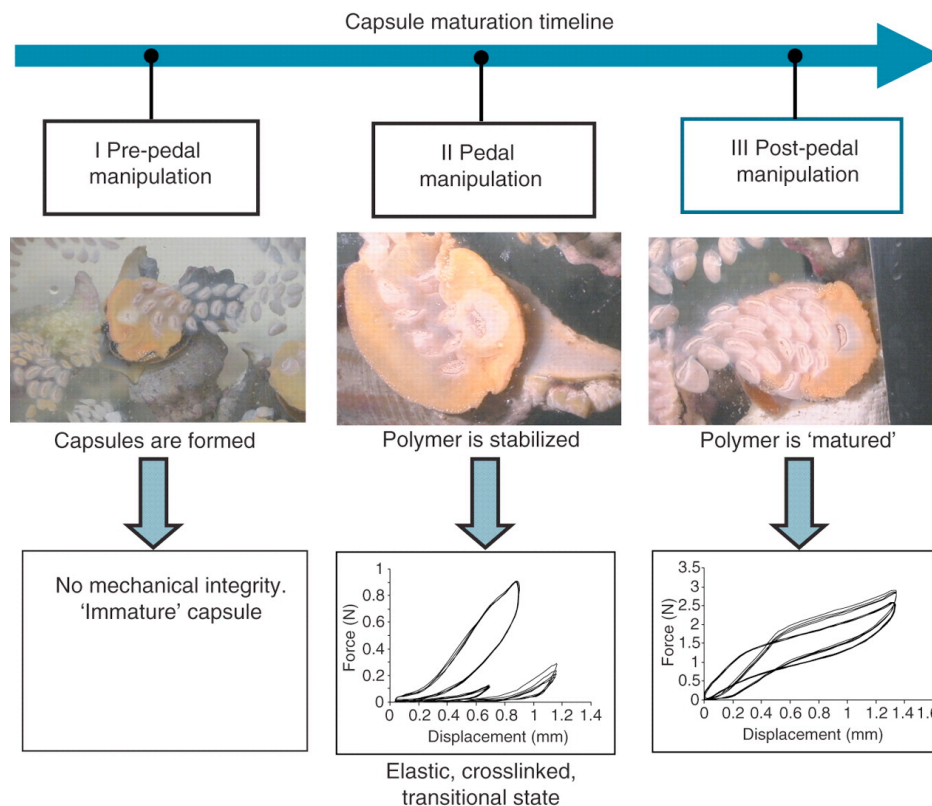


Figure 4. Development of mechanical properties in WECP. Capsule maturation is divided into three distinct phases: (I) pre-pedal manipulation, (II) pedal manipulation, and (III) post-pedal manipulation. Prior to pedal manipulation, the capsule is immature, uncrosslinked, soluble, and lacks mechanical integrity. During pedal manipulation, the ventral pedal gland (VPG) subjects the capsule to a muscular massage, and the capsule undergoes a transitional state where it is elastic and has some crosslinking. Post-pedal manipulation, the mature capsule with fully developed mechanical properties is deposited onto the substrate. Note that force scales are different in II and III. Multiple curves represent different specimens. Reproduced with permission from the Journal of Experimental Biology, Rapoport and Shadwick 2007.

1.7 A model of WECP mechanics through maturation

The awesome model for the structure and mechanics of WECP proposed by Rapoport and Shadwick (2007) starts with charge-based self-assembly of microfibrils composed of a staggered head to tail arrangement of IF-type coiled-coil protein structures. This alignment of coiled-coils is responsible for the repeat striation patterns seen in electron microscopy (Rapoport and Shadwick, 2007). The microfibrils may be interconnected, and are arranged in layers of varying orientations throughout the thickness of the material (Rapoport and Shadwick, 2007). The layers appear to be discontinuous and interdigitate with other layers, appearing to be laid down like disordered strokes of a broad paint brush (Rapoport and Shadwick, 2007). The layers do not necessarily span the entire length of the egg capsule, so tensile loading results in shearing and sliding of successive layers, leading to material failure (Rapoport and Shadwick, 2007).

Immediately following formation in the egg capsule gland, the material is soluble, white in colour, and probably held together by weak noncovalent interactions (Rapoport and Shadwick, 2007). During treatment in the VPG, the muscular massaging action brings layers of the protein closer together, at first enabling only a low density of cross-links – during this period, the material behaves like a pliant rubber (Rapoport and Shadwick, 2007).

The cross-links that form in the VPG between the coiled-coils are responsible for the heat- and strain-labile stabilization that signals the completion of the capsule maturation process (Rapoport and Shadwick, 2007). After processing in the VPG, cross-link density is sufficient to transfer mechanical stress down to the coiled-coils, which are the smallest hierarchical level of the material (Rapoport and Shadwick, 2007). The result is the Hookean region of the mechanical response, as a network of stiff coils are strained (Rapoport and Shadwick, 2007). Unraveling of the coiled-coils begins at the transition between the Hookean and yield regions, and continues throughout the yield region (Rapoport and Shadwick, 2007). However, this unraveled conformation is not stable

under physiological conditions, and the material quickly returns to its initial state once the stress is removed (Rapoport and Shadwick, 2007).

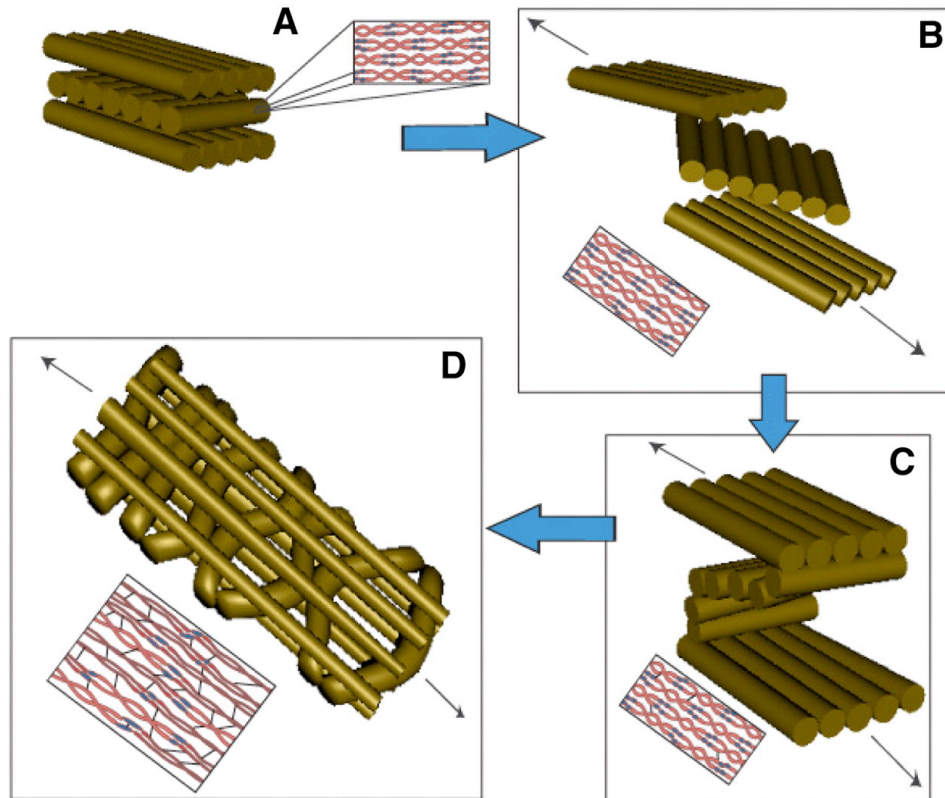


Figure 5. Model of WECP mechanics through maturation. (A) the general, uncrosslinked structure of sheets of microfibrils formed by charge-based self-assembly and laid down in varying orientations. (B) tensile loading (indicated by arrows) of the immature capsule results in shearing and sliding of the layers of sheets, leading to material failure. (C) during treatment in the ventral pedal gland (VPG), the muscular action brings successive sheets closer together, allowing crosslinks to form. (D) after processing in the VPG, the crosslink density is sufficient to transfer stresses down to the smallest hierarchical level of the material. Reproduced with permission from the Journal of Experimental Biology, Rapoport and Shadwick 2007.

Didier (2009) incorporated data from birefringence measurements and X-ray diffraction to add detail to the model at the molecular level. Birefringence decreases at the transition to the yield region, indicating a loss of overall order in the structure as α -helices are pulled apart (Didier, 2009). β -sheet signals were detected in the strained

material but the α -helices spontaneously reform on recoil, indicating that the β -sheets formed are not stable (Miserez et al., 2009).

Further evidence of the reversible α -helix to β -sheet transformation was gathered using wide-angle X-ray scattering analysis of the capsule wall during deformation (Miserez et al., 2009). Classical features of α -helices were detected at 0% strain, and a β -sheet formation was indicated at 70% strain (Miserez et al., 2009). After unloading, the X-ray diffraction pattern returns to that of an unstretched specimen, with no β -sheet features remaining (Miserez et al., 2009).

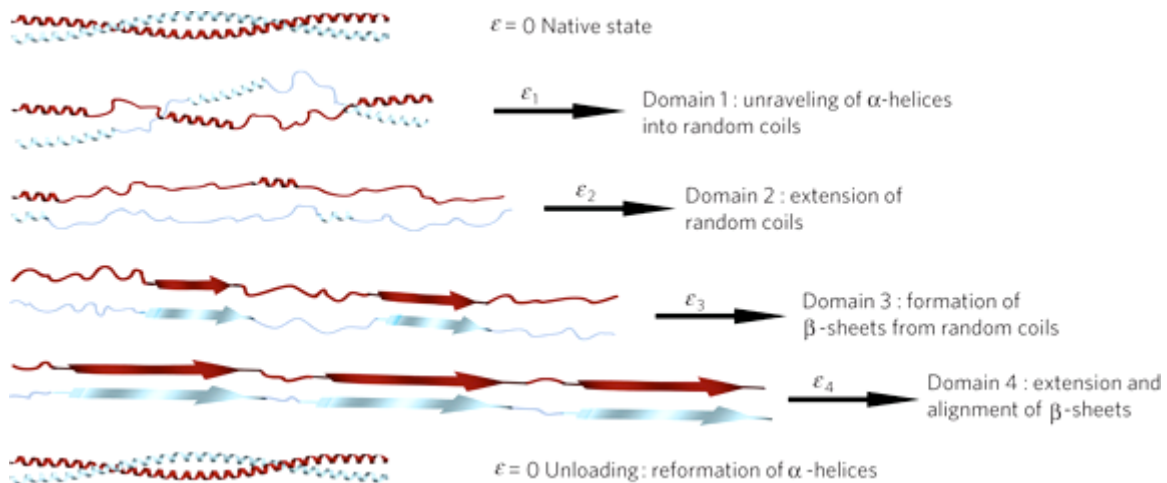


Figure 6. Reversible α -helix to β -sheet transition during straining. As the material is loaded the α -helices are pulled apart, first into random coils, then into β -sheets. Domain 1 is from 0 to 5% strain, domain 2 is from 5 to 20% strain, domain 3 is from 20 to 60% strain and domain 4 is over 60% strain. Reproduced with permission from Nature Materials, Miserez et al., 2009.

This X-ray data led to the development of a more detailed model (Figure 6) with the reversible α -helix to β -sheet transition divided up into four domains (Miserez et al., 2009). Domain 1, from unstrained to 5% strain, is dominated by α -helices. The helices begin to unfold into random coils at the yield point of the material, and a decrease in stiffness is seen (Miserez et al., 2009). Domain 2 is from 5 to 20% strain, has a lower modulus and is dominated by the extension of random coils (Miserez et al., 2009).

Domain 3 is from 20 to 60% strain, where the proportion of random coils decreases as they are replaced by β -sheets (Miserez et al., 2009). Domain 4 is β -sheet dominated, with random coils having mostly disappeared and recrystallized into β -sheets (Miserez et al., 2009). The increased modulus of domain 4 is due to the inherently stiffer nature of β -sheets, as well as their alignment along the loading axis during stretching (Miserez et al., 2009).

1.8 More mechanical properties of whelk egg capsules

Interestingly, WECP recovers Hookean behaviour in the yield region if a specimen is stretched, then held at constant strain (Rapoport and Shadwick, 2002). Stresses drop almost immediately, indicating a rapid molecular reorganization, probably due to the reformation of coiled-coils (Rapoport and Shadwick, 2007). These coiled-coils (and likely H-bonds in and among these structures) will even reform under slow continuous extension (Rapoport and Shadwick, 2007). However, the idea that coils were reforming was not supported by birefringence measurements (Didier, 2009).

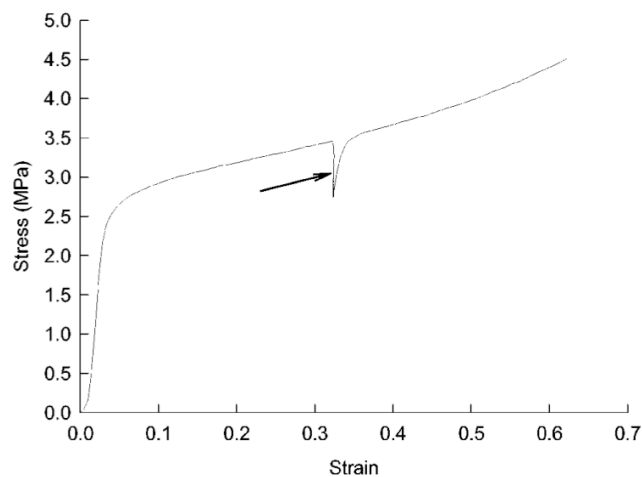


Figure 7. Stress recovery in the native capsule. The specimen was held at constant strain for 5 minutes on the extension cycle during the yield phase (arrow). Stress drops almost immediately, and the material recovers Hookean behaviour when strain is resumed, with an initial slope similar to that in the initial stiff region. Reproduced with permission from Biomacromolecules, Rapoport and Shadwick 2002.

Microscopic tests on teased-apart fibres of the egg capsule showed that the mechanical properties are intrinsic to the macromolecules, and are not due to the laminar structure of the capsule walls (Didier, 2009). Mechanical testing of microscopic fibre samples produced stress-strain curves similar to macroscopic samples, and the toe region and tertiary regions were described (Didier, 2009). The toe region precedes the Hookean region, and represents the taking up of slack in the fibrous protein matrix as the fibres are loaded (Didier, 2009). The tertiary region produced a higher modulus by pulling more directly on the primary molecular chains, beyond the point of mechanical failure in the laminar structure of macroscopic samples (Didier, 2009).

1.9 Polarized light microscopy

Polarized light microscopy is a useful technique for evaluating structure that reduces the likelihood of methodological artifacts because it does not require any physical modification of the sample. Birefringence is an optical effect generated by ordered structures on the molecular level, and can therefore be used as an index of order. There are two ways in which order produces birefringence: 1.) form birefringence, generated by the difference in refractive index between a material and the medium it is in, and 2.) intrinsic birefringence, caused by light refracting in two directions when passing through parallel structures that are closer together than the wavelength of the light. Total birefringence is the sum of the form birefringence and the intrinsic birefringence. An isotropic material should have no intrinsic birefringence, while an anisotropic (highly ordered) material should have high intrinsic birefringence (Aaron and Gosline, 1980).

Rapoport and Shadwick (2002) demonstrated that WECGP has an ordered structure with an α -helical conformation. Birefringence scans of whelk egg capsules showed that the material was highly birefringent, and that the layers of the capsule are randomly oriented (Rapoport and Shadwick, 2007). Didier (2009) showed that isolated microfibrils from the egg capsule show an increase in birefringence when they are

strained in the Hookean region, then decrease in birefringence once they are strained past the yield point, into the rubbery region.

1.10 Fourier transform infrared spectroscopy

Fourier transform infrared spectroscopy (FTIR) has been applied in the study of the molecular conformation of many different proteins, including keratin (Aluigi et al., 2008, Kreplak et al., 2004). FTIR has also been used to examine the structure and composition of other biological materials such as lipids, biomembranes, carbohydrates, and animal cells and tissues, and is used in blood and skin analysis and clinical screening tests for cervical and colorectal cancers (Stuart and Ando, 1997). FTIR has also been used to analyze drugs, wine, and artificial sweeteners (Stuart and Ando, 1997).

The infrared spectra of proteins exhibit nine absorption bands associated with their characteristic amide group, called amide A, amide B, and amides I-VII, in order of decreasing frequency. Amide A, I, and II have been used most frequently for conformational studies, and amide I is the most useful for the analysis of the secondary structure of proteins (Stuart and Ando, 1997). Amide I represents 80% of the C=O stretching vibration in the amide group (Stuart and Ando, 1997). The exact frequency of this vibration depends on the nature of hydrogen bonding involving the C=O and N-H groups, which is determined by the secondary structure of the protein (Stuart and Ando, 1997). Because proteins often have a variety of domains in different conformations, the amide I band is usually a complex composite made up of a series of overlapping component bands representing α -helices, β -sheets, turns, and random structures (Stuart and Ando, 1997).

Protein secondary structures have been assigned characteristic FTIR frequencies based on proteins that were well characterized by X-ray crystallography (Stuart and Ando, 1997). Curve fitting the amide I band gives the fractional areas of the component bands, which are directly proportional to the relative amounts of the secondary structure they

represent (Stuart and Ando, 1997). The percentages of α -helices, β -sheets, and turns are estimated by adding the areas of all the component bands assigned to those structures, and then expressing the sum as a fraction of the total amide I area (Stuart and Ando, 1997).

The secondary structure of electrospun WECGP was of interest because the current model has a network of coiled-coils as the smallest hierarchical level of the native capsule material (Rapoport and Shadwick, 2007). Straining of the coiled-coils results in the Hookean region of the mechanical response, unraveling of the coils results in the rubbery yield region, and reformation of the coils enables the material to recover once stress is removed (Rapoport and Shadwick, 2007). For the electrospun fibres to have similar mechanical properties to the native capsule, it follows that the secondary structure should also be similar.

1.11 An introduction to biomimetics and electrospinning

The development and fabrication of new materials based on biological models (biomimetics) is of broad scientific, medical, and industrial interest. Because biomaterials are synthesized at ambient temperatures and in aqueous conditions using highly specialized molecules, they have enormous potential for the design of new materials. With self-assembly, materials can be produced with less energy and less dependence on fabrication machinery or environmentally damaging processing steps. As the culmination of millions of years of natural mechanical design, biomaterials offer a wealth of information and a great opportunity for materials design and biomimetic applications.

Electrospinning is a novel technique that produces micro- and nano-scale fibres by applying a high voltage electric field to a solubilized polymeric solution. Electrospinning has been successfully applied to many synthetic polymers, as well as naturally biosynthesized protein polymers such as silk, collagen, elastin, and keratin (eg. Aluigi et

al., 2008; Chen et al., 2007; Li et al., 2005; Matthews et al., 2002; Sukigara et al., 2003, 2004, and 2005). The whelk egg capsule protein seemed an ideal candidate for this technique.

Electrospun fibres have great potential for materials design and biomimetic applications. Electrospinning has emerged as a leading technique for generating biomimetic scaffolds for tissue engineering. The ultra-fine fibre scaffolds produced closely mimic the topology of the extracellular matrix, and cells attach and proliferate on the scaffolds (Li et al., 2006; Min et al., 2004). Other applications for electrospun nanofibres include wound dressing materials, membrane filters, aerosol filters, textile composites, drug delivery, biological membranes, artificial blood vessels for vascular grafts, formation of carbon nanotubes, and production of electrically conducting or insulating nanofibrous material. Ultimately, the goal of this project is to be able to fabricate self-assembling elastomeric biomaterials with useful tensile properties based on the molecular design of the whelk egg capsule.

1.12 History of electrospinning

Creating fibres by electrifying a fluid can be traced back to the late 1800's, when electrostatic machines were available in many laboratories (Reneker and Fong, 2006). J. Zeleny published a paper in 1917 that described the observation of liquid jets created by electrical forces (Zeleny, 1917), but the observation of these jets is much older. G.I. Taylor wrote that W. Gilbert observed in about 1600 that a drop of water on a dry surface is drawn up into a cone when a piece of charged amber is held above it (Taylor, 1969).

Electrospinning as a technique to make fibres was first patented by A. Formhals in 1934 (US patent 1,975,504). This followed research in the 1920's that established that polymers are long linear molecules (Reneker and Fong, 2006). Formhals envisioned electrospinning as a technique for making textile fibres, but the textile industry came to use other methods (Reneker and Fong, 2006).

Despite further publications and patents issued from the 1930's to 1990, interest in electrospinning only developed in the 1990's, along with broad interest in nanotechnology and nanomaterials in general (Reneker and Fong, 2006). Electrospinning is now being applied to materials science as an efficient method to manufacture micro- and nano-sized fibres of many polymers.

Several aspects of electrospinning nanofibres make the process appealing. The equipment required for electrospinning is simple, not overly expensive, and readily available. Nanofibres have a very high surface area to volume ratio, which is key to many of their applications. The process is reproducible, although obtaining a uniform fibre diameter and collecting the fibres can be problematic. Electrospinning also offers a simplified manufacturing process, allowing a microporous structure to be sprayed directly onto a substrate, such as a fabric, screen, or living tissue (Schreuder-Gibson and Gibson, 2006). The electrospinning process does not involve extreme temperatures, enabling the addition of temperature sensitive components such as drugs and biological materials (Schreuder-Gibson and Gibson, 2006).

Parameters such as concentration, field strength, and distance between the source and collector influence the size and consistency of the spun fibres. These parameters must be optimized for reliable fibre formation and in order to produce suitable specimens for tensile testing and other applications. Less than optimal electrospinning parameters produce fibres of non-uniform diameter, droplets instead of fibres, or "beads on a string" - droplets connected by fibres.

1.13 The electrospinning technique

The electrospinning apparatus is composed of three main components: a high voltage generator, a syringe feeding the polymer solution to a capillary tip, and a collector.

Electrospinning occurs in three stages: 1.) jet initiation, 2.) jet elongation, and 3.) jet solidification or fibre formation. During the jet initiation stage, electrostatic forces overcome the surface tension of the polymer solution. The charge induced on the polymer solution deforms the spherical drop on the capillary tip to a conical shape, called a Taylor cone. At a critical voltage, charge imbalance results in the formation of an electrically charged jet. The jet is emitted from the capillary tip towards the electrically grounded collector.

The jet will remain stable over a certain distance, where it will travel in a straight line. Then it becomes unstable, bends, and follows a looping, spiral course. Jet elongation occurs during this unstable, looping travel, when electrical forces stretch the jet to thousands to millions of times its original length (Fang et al., 2006). The charges in the jet are evenly distributed and repel each other, contributing to elongation (Fang et al., 2006). Solvent evaporation occurs throughout jet initiation and elongation, further decreasing the diameter of the jet.

The final stage of jet solidification occurs when the viscosity of the polymer solution becomes so great that there is no further elongation of the jet (Fang et al., 2006). The result is the deposition of a single continuous fibre filament on the collector (Yamashita et al., 2007). Both the stretching and the accompanying evaporation of the solvent cause a reduction in the diameter of the jet and therefore of the fibres collected. The dried fibres are deposited either randomly or in an aligned manner on the surface of the collector.

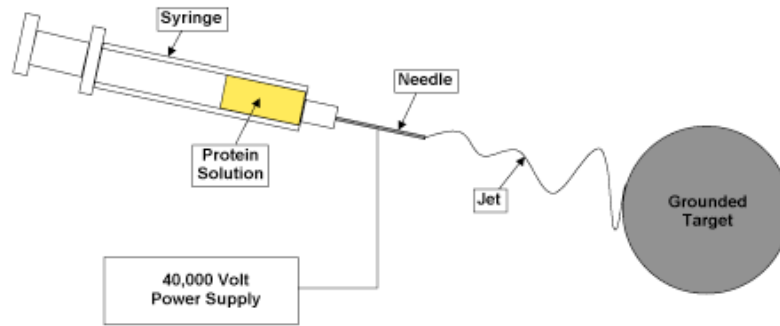


Figure 8. Whelk egg capsule gland protein is solubilized and placed in a syringe with a flat-tipped needle. When a high voltage is applied, the electrical forces overcome the surface tension of the solution at the needle tip. This results in the formation of a jet, which travels from the needle to a grounded target.

1.14 Electrospinning parameters

The characteristics of electrospun fibres depend on both the properties of the polymer fluid (concentration, viscosity, conductivity, surface tension) and on the operating conditions of the electrospinning process (distance between capillary tip and collector, flow rate, strength of electric field, bore diameter of needle, rate of deposition). Electrospinning solvents should be highly volatile to ensure that polymeric nanofibres are deposited dry on the collector to prevent resolubilization. Formic acid was chosen for its volatility and convenience – it leaves no residual salt when it evaporates and it effectively solubilizes WECGP.

The electrospinning process uses an electric field to control the formation and deposition of polymers on a grounded target. The distance between the polymer solution source and the target can be increased to ensure complete evaporation of the solvent so that electrospun fibres are deposited dry on the collector and do not resolubilize upon deposition. Yang (2006) found that increasing the distance from the needle to the target does not necessarily enhance solvent evaporation, but does reduce the electric field strength. These two parameters should therefore be considered together.

Katti et al. (2004) refer to the two parameters together as the electrospinning voltage, measured in kV/cm. They found that the diameter of the electrospun fibres decreased with an increase in electrospinning voltage (Katti et al., 2007). Above 1 kV/cm there was no significant change in fibre diameter (Katti et al., 2007).

Higher gauge (smaller bore diameter) needles were found to produce smaller diameter nanofibres (Katti et al., 2007). The difference was significant between 16 and 20 gauge needles (internal diameters of 1.19 mm and 0.58 mm, respectively), but there was no significant difference between 18 and 20 gauge needles (internal diameter of 18 gauge is 0.84 mm) (Katti et al., 2007).

Poly(ethylene oxide) (PEO) is often added to the electrospinning solutions to enhance fibre formation. PEO is a soluble synthetic polymer known for its ease of processing in electrospinning applications. Like most polymers, PEO solutions must reach a certain critical concentration before electrospinning will produce continuous fibres. If the solution is too dilute, droplets result, and if it is too concentrated, the solution becomes too viscous to undergo the plastic stretching necessary for fibre formation (Gupta, 2004).

The density of electrospun fibres deposited on the collecting target was found to increase linearly with time, indicating a uniform rate of deposition (Katti et al., 2007). However, as the fibre size becomes very small, the yield of the electrospinning process becomes very low. This is the major technical barrier for scale-up processing, such as manufacturing electrospun fabrics for clothing (Fang et al., 2006). Another major technical problem for mass production is the assembly of spinnerets. Straightforward multi-jet arrangements cannot be used because adjacent electrical fields tend to interfere with each other (Fang et al., 2006). Issues with increasing the product yield have held electrospinning back from many industrial applications in the past, but increased interest in nanotechnology raises expectations for the future.

1.15 Hypothesis

Enough was already known about the biology of the whelk egg capsule protein to make some predictions about what would happen when the electrospinning technique was applied to the immature, solubilized protein. We knew it was unlikely that electrospinning alone would yield the mature protein, since there is nothing in the technique to act in place of the hour-long muscular massage that the egg capsules receive in the VPG. We knew from the maturation timeline that a transitional state exists between the immature and the mature protein, and that the electrospun fibres would at best be in a similar state. If they were, we planned to introduce a cross-linking step to take the fibres closer in their mechanical properties to the mature protein.

2 Methods

2.1 Preparation and characterization of the blend solutions

Adult female whelks (*Busycon canaliculatum*) were dissected and their nidamental glands removed. Glands not used immediately were stored at -80°C . Glands were placed in a solution of 25 mM TCEP (Alfa Aesar, Ward Hill, MA, lot # E25R045, MW 286.65) in 88% formic acid and homogenized using a glass mortar and pestle. WECGP was solubilized and subsequently dialyzed against 0.01 M acetic acid in Spectra/Por molecularporous membrane tubing (molecular cut off 3,500) for 5 days at 4°C . The dialysis solution was replaced daily and was on a stir plate on low setting. The solution was then freeze-dried for 3 days in a Labconco FreeZone 4.5 to obtain the purified protein.

Blend solutions were prepared by first adding 25 mM TCEP to 88% formic acid, then adding the freeze-dried protein to make an 8 wt% WECGP solution. Poly(ethylene oxide) (PEO, MW 300,000 from Alfa Aesar) was added directly to the 8 wt% WECGP solution in order to obtain 2 wt% PEO, and 10 wt% total polymeric concentration. The same protocol was used to make blend solutions of other concentrations.

2.2 Selection of TCEP as the reducing agent

The egg capsule gland was obtained by dissecting the gland out of an adult female. The gland was homogenized in 6 M guanidine solution using a glass mortar and pestle and centrifuged for 30 minutes at 13500 rpm. The supernatant was then dialyzed against 0.01 M acetic acid for 24 hours in Spectra/Por dialysis tubing (Spectrum Labs, MWCO 3500) and freeze-dried.

A stock solution of freeze-dried WECGP in double strength sodium dodecyl sulphate polyacrylamide gel electrophoresis (SDS-PAGE) sample buffer (10 mg/ml) was

produced. Solutions of 0.5 and 20 mM ethylenediaminetetraacetic acid, disodium salt dehydrate (EDTA, BioRad), 0.5 and 20 mM mercaptoethanol (Sigma), 0.5 and 20 mM dithiothreitol (DTT, Sigma), and 0.5 and 20 mM TCEP (Alfa Aesar) were prepared using the protein/buffer solution. The stock solution was used as a control. 5 μ l samples of all solutions were separated on a 14% gel, run at a constant current of 25 mA. Molecular weights were determined with a broad-range protein standard (Benchmark Pre-Stained Protein Ladder).

Another stock solution of freeze-dried WECGP in double strength SDS-PAGE sample buffer (10 mg/ml) was produced and used as a control. Different amounts of TCEP or DTT were added to the protein/buffer solution, resulting in solutions with 5, 10, 25, and 50 mM TCEP and 0.5 and 20 mM DTT. 5 μ l samples of all solutions were separated on a 14% gel, run at a constant current of 25 mA. Molecular weights were again determined with a broad-range protein standard (Benchmark Pre-Stained Protein Ladder).

2.3 Nanofibre electrospinning and properties

All fibres were generated using the NEU-010 Nanofibre Electrospinning Unit (Kato Tech Co., Ltd. Kyoto, Japan, Figure 10), and all experiments were carried out at room temperature. The syringe cradle of the NEU-010 was built for 20 ml syringes, but 1 ml syringes were used in this study. The machine was adapted to accommodate the smaller syringes by adding an extending block to the syringe pump.

About 0.5 ml of blend solution was loaded into a 1 ml syringe linked to a blunt-tipped needle (18 gauge, inside diameter 0.84 mm). The anode of the 40 kV power supply was connected to the metal needle. The cathode (collecting screen) was a rotating stainless steel cylinder of 8.5 cm diameter. The target mandrel was not rotating and traverse movement was shut off in order to concentrate the sample in a small target area.

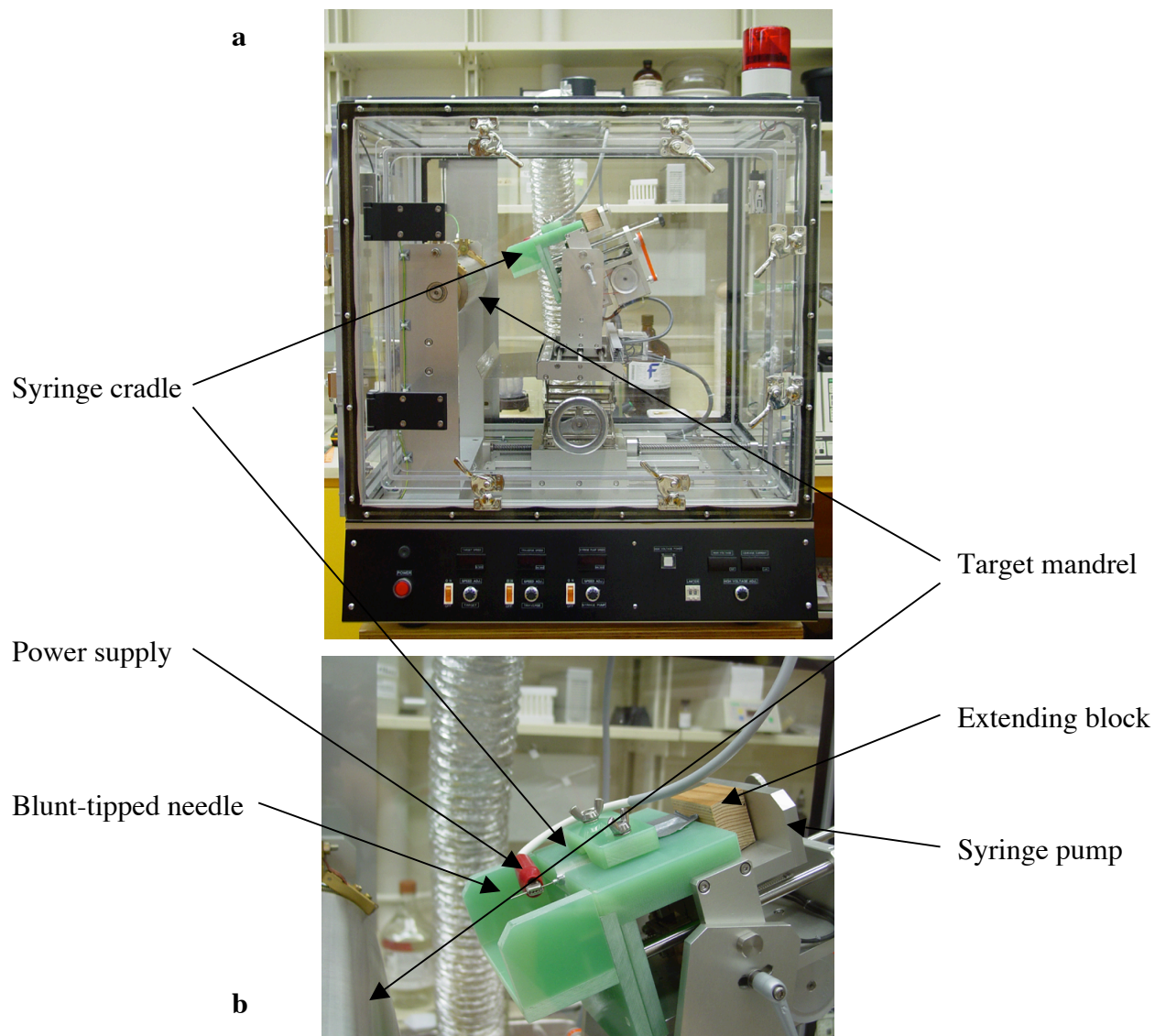


Figure 9. (a) The Kato Tech NEU-010 Nanofibre Electrospinning Unit. The apparatus holding the syringe cradle and pump has been adjusted to maintain a set distance of 10 cm between the source needle and the cylindrical target mandrel. (b) Closer view of syringe cradle and extending block attached to the syringe pump to accommodate the 1cc syringes used in this study. The anode of the power supply is also visible, clipped to the blunt-tipped needle.

The target mandrel was covered with an aluminum sheet to obviate the task of removing the electrospun samples. The foil allowed the target surface to remain suitably grounded. A voltage of 20 kV was applied and a constant volume flow rate of 0.2 ml/min was maintained. The collecting screen was placed at a distance of 10 cm from the syringe tip to ensure the complete evaporation of the solvent.

2.4 Preparation of SEM samples

Nanofibres were collected on the aluminum sheet as non-woven mats of randomly oriented fibres. The fibres adhered to the sheet and were not easily removed. Weak acid, weak base, distilled water and ethanol solutions had no effect on fibre adhesion. The aluminum sheet with the nanofibres deposited on the surface was therefore cut and mounted directly on aluminum SEM specimen stubs with silver adhesive solution. Later samples were electrospun directly onto SEM specimen stubs, which were attached to the target mandrel through punctures in the aluminum foil. This method resulted in easier imaging due to a smaller range of fluctuations in the height of the specimen.

2.5 Collection of SEM images

Nanofibre morphology was examined by scanning electron microscopy using a Hitachi S-4700 Field Emission SEM with an acceleration voltage of 1.0 kV and working distance of about 4mm. At this acceleration voltage the S-4700 is capable of 2.5 nm resolution.

Samples on SEM specimen stubs were viewed uncoated, or sputter coated with 4 ± 1 nm of gold using a Cressington Sputter Coater 208HR and a Cressington Thickness Controller mtm20 (Cressington Scientific Instruments, Watford, England). Uncoated samples tended to melt when exposed to the electron beam for any length of time, making them difficult to image. Coated samples were more durable and therefore were used for imaging and measurements.

Charging was observed when visualizing many of the samples. Diameter of the fibres, interconnectedness of the fibres, thickness of the fibre mat, attachment of the mat to the specimen stub, and concentrations of the blend solutions could all affect charging of the samples.

2.6 Polarized light microscopy

Blend solutions as described above were electrospun and collected on a modified target. 6 mm by 6 mm windows were cut in the aluminum foil that was wrapped around the target mandrel, and glass microscope slides were attached behind the windows. Electrospun fibres seek a grounded target, so many of the fibres spanned the window in the foil and were suspended above the slide, but some fibres were collected and observed, and photographed in air using plane polarized light.

Birefringence measurements were taken on smaller samples of fibres using a Wild Senarmont 546 compensator with a 546nm interference filter. These fibres were suspended freely from the target mandrel. They were collected by very gently lifting them onto a drop of immersion oil on a piece of cover slip.

Birefringence is the angle of retardation, or how much the sample rotates the plane of polarized light, divided by the path length, or thickness of the sample. Retardation had been calibrated for the scope as:

$$\Gamma = \theta * 3.03 \text{ nm/deg}$$

where Γ is the optical retardation, measured using a Senarmont $\lambda/4$ compensator plate, and θ is the degree of rotation. Birefringence is then calculated as:

$$\text{Birefringence} = B = \frac{\Gamma}{t}$$

where Γ is the retardation and t is the thickness of the sample.

2.7 *Determining the effect of PEO addition*

PEO was added to 88% formic acid to produce solutions of 2 wt%, 3 wt%, 4 wt%, 5 wt%, and 10 wt%. These solutions were electrospun using the same parameters and protocol described above for the blend solutions. The solutions that formed fibres had the fibre diameters measured according to the protocol described below for the series of blend solutions.

PEO is highly soluble in water. Therefore, rinsing with water was considered adequate to wash away any PEO that was not bound or incorporated into fibres. Samples were imaged on the SEM, washed, and imaged again. SEM specimen stubs that were subjected to washing with water all had samples electrospun directly onto the stubs and were not sputter-coated. Stubs were thoroughly rinsed with distilled water and allowed to air dry. They were then dried further under vacuum before being transferred to the SEM specimen chamber. Diameters of the fibres were measured and washed samples compared to the pre-washed samples.

2.8 *Measurement of electrospun fibres*

Two concentration series of blend solutions were imaged and measured for fibre diameter, one with a constant weight percent of protein (A-D) and one with a varying amount of protein (D-G). All blend solutions contained 25mM TCEP and used 88% formic acid as the solvent.

Images were collected at 500 times and 5000 times magnification for overall images, and 10,000 times, 25,000 times, and 50,000 times magnification for measurement. The 25K images were preferred for measurement since that magnification had more fibres available for measurement than the 50K images, and created less measurement error than the 10K images. However, good quality 10K and 50K images were used when necessary in order to collect enough measurements.

Stub A	8 wt% WECGP	5 wt% PEO
Stub B	8 wt% WECGP	4 wt% PEO
Stub C	8 wt% WECGP	3 wt% PEO
Stub D	8 wt% WECGP	2 wt% PEO
Stub E	7 wt% WECGP	3 wt% PEO
Stub F	6 wt% WECGP	4 wt% PEO
Stub G	5 wt% WECGP	5 wt% PEO

Table 1. Blend solution concentration series used for producing electrospun fibres for diameter measurement.

Diameters of the nanofibres were acquired from SEM images of random locations on the specimen stubs, using the image analysis software ImageJ (National Institute of Health). The SEM images selected for measurement were zoomed in to 200% for analysis. All images were calibrated using the built-in scale bar from the SEM image as a known distance. For each sample the diameter distribution was evaluated from 100 measurements. All fibres measured were within the field of focus, and had visible and distinct edges. Fibre orientation in the field of view was irrelevant, and fibres that met the criteria were randomly selected for measurement.

2.9 FTIR spectroscopy

To investigate the composition of the electrospun fibres, FTIR spectra were obtained using a Nicolet 6700 FTIR using the provided OMNIC software suite (Thermo Scientific, Waltham, MA, USA). Data was acquired from solid samples of PEO, freeze-dried WECGP, and electrospun fibres from a blend solution of 8% WECGP and 2% PEO (solvent was 88% formic acid with 25mM TCEP). Samples were clamped directly into the Nicolet 6700 without treatment or coating, maintaining the integrity of the solids.

Frequency (cm-1)	Assignment
1621-1640	β -structure
1641-1647	Random coil
1651-1657	α -helix
1658-1671	Turns and bends
1671-1679	β -structure
1681-1696	Turns and bends

Table 2. Characteristic amide I band frequencies of protein secondary structures. These characteristic frequencies were used to determine the positions of the peak intervals in the curve-fitting procedure. From Stuart and Ando, 1997.

The amide I band (1600-1700 cm^{-1}) of each spectrum was subjected to a curve fitting procedure using six Gaussian distributions centred at the frequencies of well-characterized secondary structures (Stuart and Ando, 1997). During the fitting the peak heights were not constrained, but the peak positions were kept to a limited interval. Integrating the area of each peak and then normalizing it to the total area of the amide I band determined the contribution of each peak to the amide I band. The fitting procedure was done using Microsoft Excel and the peak fitting module of the OriginPro 8.1 software package (OriginLab, Massachusetts, USA).

2.10 Preparation of electrospun samples for mechanical testing

Testing the mechanical properties of a single electrospun fibre would be ideal but is unrealistic without an omnipotent technician. Fibres were therefore measured as thick, semi-aligned non-woven mats. Since fibres spun onto aluminum foil on the collecting mandrel proved all but impossible to remove, mats spanning the gap between two insect pins that protruded perpendicularly from the target mandrel were used (Figure 11).

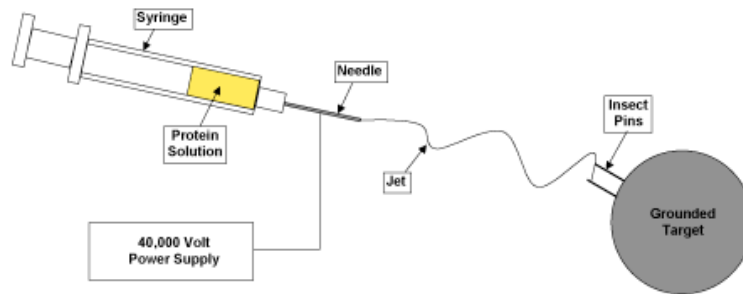


Figure 10. Modified electrospinning apparatus for collection of samples for mechanical testing. Two insect pins were mounted beneath the aluminum foil that covers the target mandrel. The pins protruded perpendicularly from the mandrel, pointing towards the source needle. Electrospun fibres spanned the gap between the pins, avoiding deposition upon and adhesion to the foil.

Electrospun protein blend fibres were collected from the gap between the insect pins and either immediately fixed to the mechanical testing apparatus, or subjected to a cross-linking step first. The cross-linking procedure was simple submersion of the sample in a 1.25% glutaraldehyde solution for a period of 1 hour. At the end of the hour the sample was removed and allowed to air dry for 24 hours before being fixed to the testing apparatus. Other samples were immediately fixed to the apparatus, tested, and then subjected to the cross-linking step while still mounted in the testing apparatus.

A sample of 7 wt% PEO in formic acid was electrospun for mechanical testing to determine whether it could contribute to the mechanical properties of fibres from the protein blend solutions. This was spun directly onto aluminum foil on the target mandrel. PEO does not adhere to the foil as strongly as WECGP and can be removed as a thick mat using a razor blade. A pair of razor blades, fixed together to cut 7.0 mm sections, was used to cut test-sized strips of width $7.0 \text{ mm} \pm 0.1 \text{ mm}$ and length $12.0 \text{ mm} \pm 0.1 \text{ mm}$. The strips were measured using Vernier calipers. Thickness was measured using a digital micrometer, and ranged from 0.300 to 0.450 mm, $\pm 0.005 \text{ mm}$.

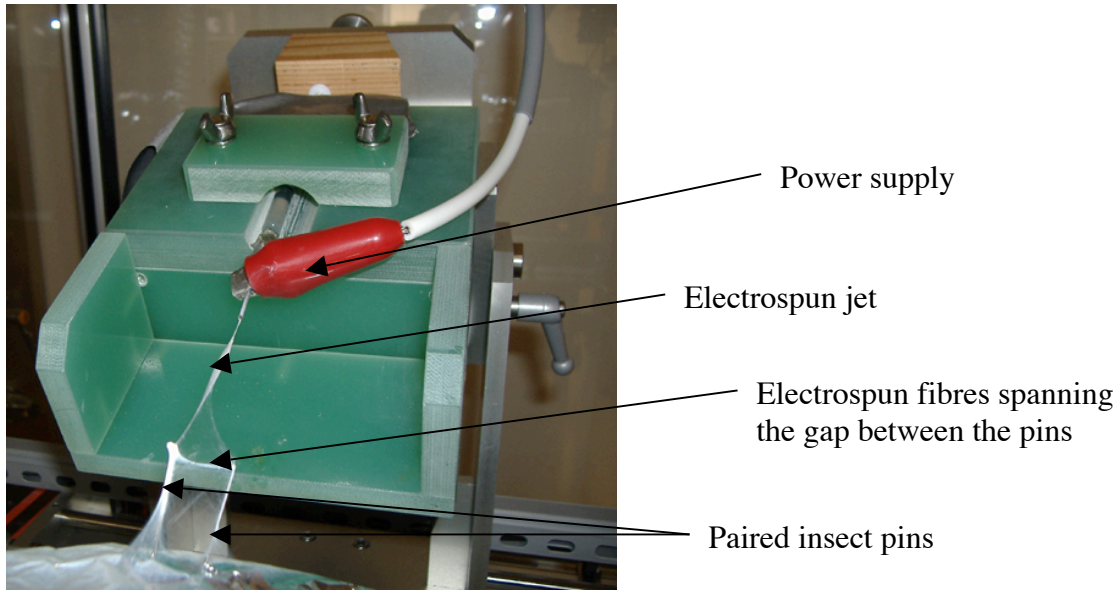


Figure 11. Electrospun fibres that spanned the gap between two insect pins were collected for mechanical testing.

2.11 Mechanical testing apparatus

The mechanical properties of the mat samples were tested using a microscope-based micro-tensile tester (Figure 12). The apparatus was originally developed by Gosline et al. (1995) for use on hydrated spider silk fibres, which are usually only microns in diameter and require extremely small forces to test. The apparatus uses thin glass rods as force sensing elements. The rods are mounted on microscope slides and force is determined by measuring the deflection in the beam using a video dimension analyzer attached to the microscope. The micro-tensile tester is capable of measuring nano-Newton forces when using very thin glass beams (Savage et al., 2003).

Beam theory is used to convert the deflections of the beam into force values:

$$\text{Force} = F = \frac{3xEI}{L^3}$$

where x is the stretch of the sample, E is the Young's modulus of glass ($5.72 \pm 0.06 \times 10^{10}$ N/m², Fudge et al., 2003), I is the second moment of area of the beam (bending moment), and L is the length of the beam (Fudge et al., 2003). Force and deflection have a linear relationship for beam deflections up to approximately 10% of the length (Fudge et al., 2003), so glass micro-beams were chosen to minimize deflection during a test.

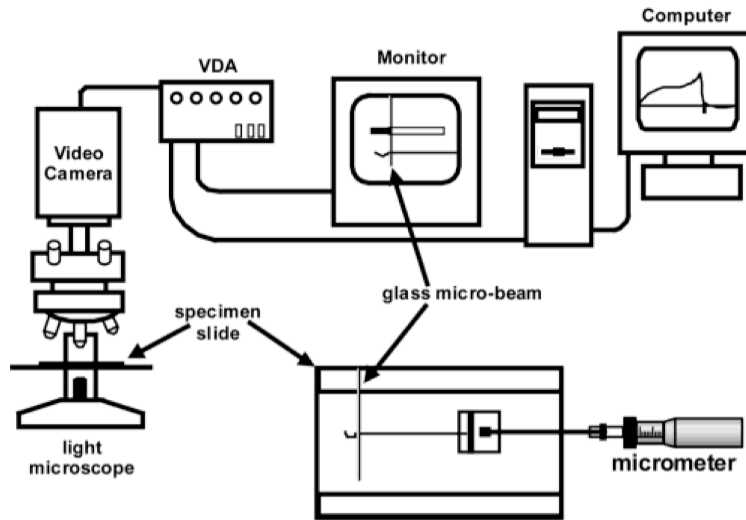


Figure 13. The microscope-based micro-tensile testing apparatus used to measure force in electrospun samples. A video dimension analyzer (VDA) tracked the movement of the glass micro-beam. Reproduced with permission from Biomacromolecules, Savage et al., 2003.

The diameters of the glass beams were slightly tapered instead of perfectly constant. For a uniformly tapered cylinder the second moment of area is:

$$I = \frac{\pi (r_1)^3 (r_2)}{4}$$

where r_1 is the radius at the point where the beam is fixed, and r_2 is the radius at the point where the sample is attached (Fudge et al., 2003).

Samples electrospun to span the gap between two insect pins were glued with 24 h epoxy (J.B. Weld) to the glass micro-beam at one end and to a moveable cover slip on the

other. The cover slip was attached to a micrometer mounted under the microscope. A video camera (Panasonic WV-BL600) was mounted on the microscope and connected to a video dimension analyzer (VSA-303, PIM, San Diego, USA), which tracked the deflection of the micro-beam. The VDA generates an electronic window that can follow the movement of the contrast boundary created by the edge of the glass rod, and provided voltage outputs that are proportional to the movement of the rod. A monitor (Panasonic Colour Video Monitor CT-133/YC) was used to follow the deflection of the glass beam. The stretch of the sample was isolated for each point by subtracting the deflection of the beam from the movement of the micrometer.

The specimen slide had a water chamber surrounding the micro-beam and cover slip, which was filled with distilled water before testing to keep the sample hydrated and completely submerged. Prior to testing, the sample length and width, the beam length and diameter at the fixed point and sample attachment point were all measured using a filar micrometer eyepiece. The microscope system was calibrated with a calibration slide with 0.01mm increments (Bausch and Lomb, USA).

2.12 Mechanical testing procedure

It is not simple to perform accurate measurements of tensile properties of nanofibre mats because of the intrinsic weakness and difficulty to manage this kind of material. With patience, stoicism, and stubborn pig-headedness, measurements were repeated successfully on 6 different samples. Handling of the samples was kept to a minimum.

Samples ranged from 1.87 to 3.68 ± 0.05 mm in length, and 0.493 to 0.243 ± 0.05 mm in width. Width and thickness of the samples was not uniform. Thickness could not be measured directly once the sample was mounted and so was estimated by eye as one quarter of the width.

Once firmly attached to the testing apparatus, samples were extended in 20 μm increments starting at slack length. Samples were subjected to one of the following treatments: 1.) extension until material failure, 2.) extension to a set point then a

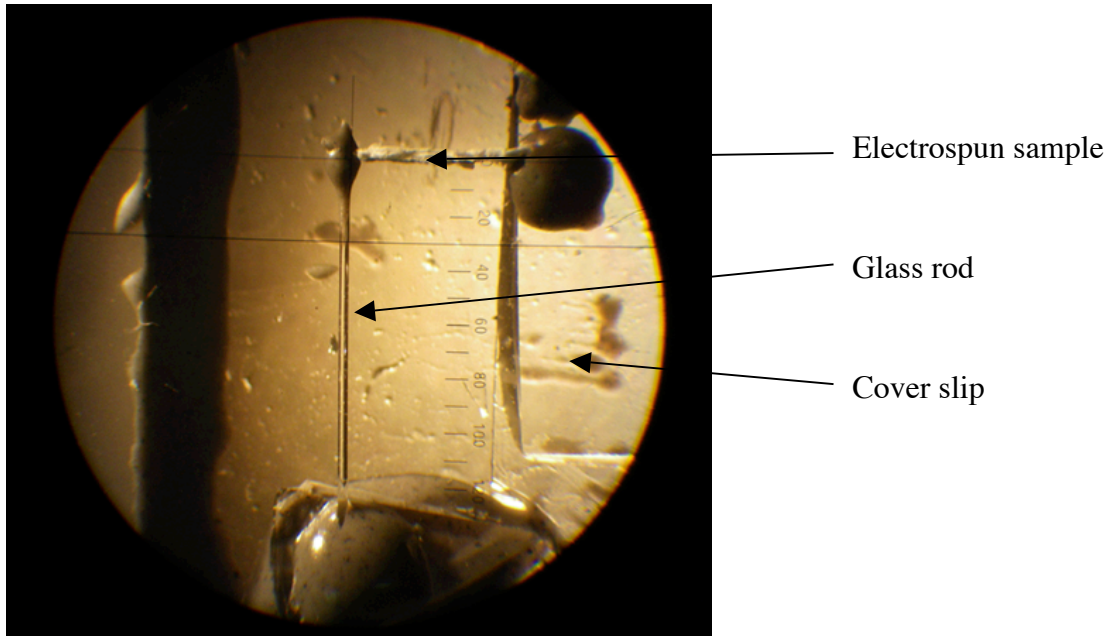


Figure 13. Electrospun samples were glued to a glass micro-beam at one end and a cover slip attached to a micrometer on the other.

controlled recoil to get a hysteresis loop, or 3.) hold for a set time during extension before continuing the hysteresis loop. In materials testing, hysteresis is the proportion of strain energy that is lost by damping through viscous interactions within the material.

Force was recorded in mN and converted to engineering stress ($\text{MPa} = 10^6 \text{ N/m}^2$) using the estimated cross sectional area of the sample:

$$\text{Stress} = \sigma = \frac{F}{A}$$

where F is force in Newtons and A is the cross sectional area in square meters.

Strain was calculated using the formula:

$$\text{Strain} = \varepsilon = \frac{(L - L_0)}{L_0}$$

where L is the measured length of the sample and L_0 is the original length of the sample. Stress-strain curves were generated from the data using Microsoft Excel and SigmaPlot. The initial Young's modulus was calculated for each stress-strain curve by finding the initial slope. Hysteresis was calculated for each stress-strain curve by taking the ratio of the area under the extension curve to the area under the relaxation curve.

3 Results

3.1 *The effect of TCEP addition*

Phosphines selectively reduce disulphide bonds and are essentially non-reactive toward other common protein functional groups. TCEP was chosen as a reducing agent because it is odorless, non-volatile, resistant to air oxidation, and able to reduce disulphide bonds at low pH. SDS-PAGE was used in order to test the efficacy of TCEP in comparison to DTT, which was used in earlier work on WECGP (Rapoport, 2003). The gel showed that at 25 mM TCEP, disulphide bonds in the protein were completely reduced and the WECGP was broken down into its 50 kDa monomer. This was similar to the effect of 20 mM DTT, shown by Rapoport (2003) to fully break down the protein into its monomeric subunit. The same amount of protein was applied to all gels, but without the addition of reducing agents such as TCEP or DTT, WECGP does not travel far past the 5% stacking gel (Figure 14). The decreased amount of protein visible in the lanes without reducing agents shows that the large molecular weight protein aggregates were too large to enter the 14% running gel.

All WECGP electrospinning blend solutions contained 25 mM TCEP in order to break the protein down into its monomeric 50 kDa subunit. Without the TCEP, the WECGP solution was difficult to homogenize, tended to aggregate, and did not form fibres.

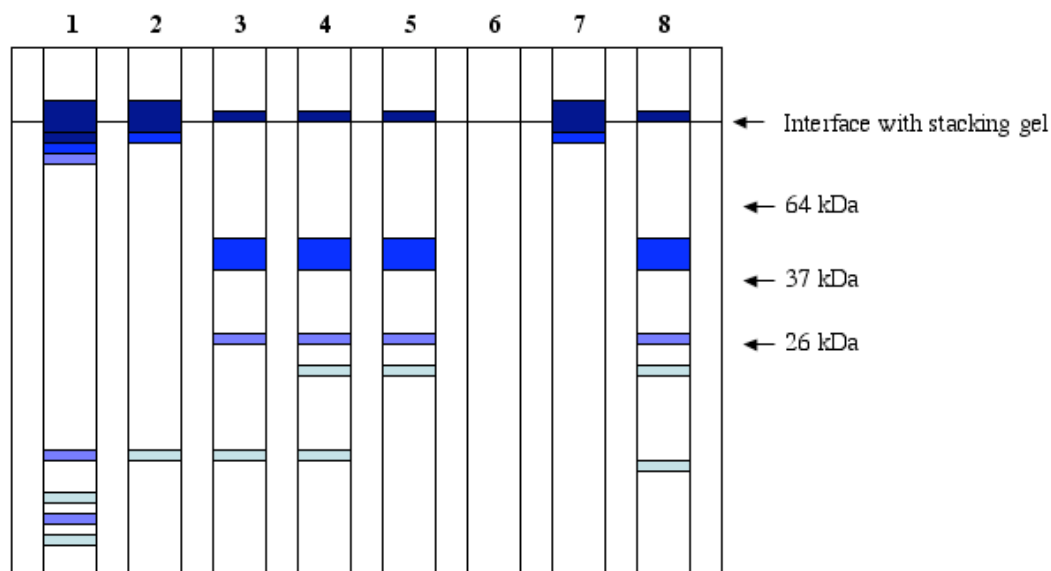


Figure 14. Diagram of SDS-PAGE gel showing the effect of several concentrations of TCEP and two concentrations of DTT on the breakdown of WECGP to its 50 kDa monomer. Lane 1 is the marker, lane 2 is 5 mM TCEP, lane 3 is 10 mM TCEP, lane 4 is 25 mM TCEP, lane 5 is 50 mM TCEP. Lane 6 was left empty. Lane 7 is 0.5 mM DTT, a concentration insufficient for monomer formation, and lane 8 is 20 mM DTT, a concentration sufficient for complete breakdown of the protein into its 50 kDa monomer. A TCEP concentration of 25 mM or greater has a comparable effect to 20 mM DTT and is therefore also considered sufficient for complete breakdown into the monomeric subunit.

3.2 *The effect of electrospinning parameters*

Electrospinning was attempted at distances of 5 – 30 cm, in increments of 5 cm, with applied electric field strengths of 5 – 40 kV, in increments of 5 kV. At distances longer than 15 cm, fibres were not reliably deposited on the target and extensive and tedious cleanup of the equipment was required. Field strengths greater than 30 kV caused the electrospun jet to fluctuate wildly at any distance.

At distances shorter than 5 cm a spark was discharged, indicating breakdown of the electric field between the charged syringe needle and the grounded target. Field strengths lower than 15 kV deposited wet material on the collecting mandrel, resulting in unattractive blobs of resolubilized protein, and no fibres (Figure 15 b). The “beads-on-a-string” fibre morphology was produced as the electric field approached the optimum

strength for fibre formation (Figure 15 c). Voltage polarity was not altered during the course of the experiments.

Syringe pump speeds over several orders of magnitude were attempted, from 10 ml/h down to 0.01 ml/h. A greater pump speed is desirable to enhance the rate of fibre production, but only very slow speeds were successful in producing uniform nanofibres. Higher speeds deposited wet material on the target mandrel, forming films or blobs of resolubilized protein similar to those produced at inadequate field strengths (Figure 15 a).

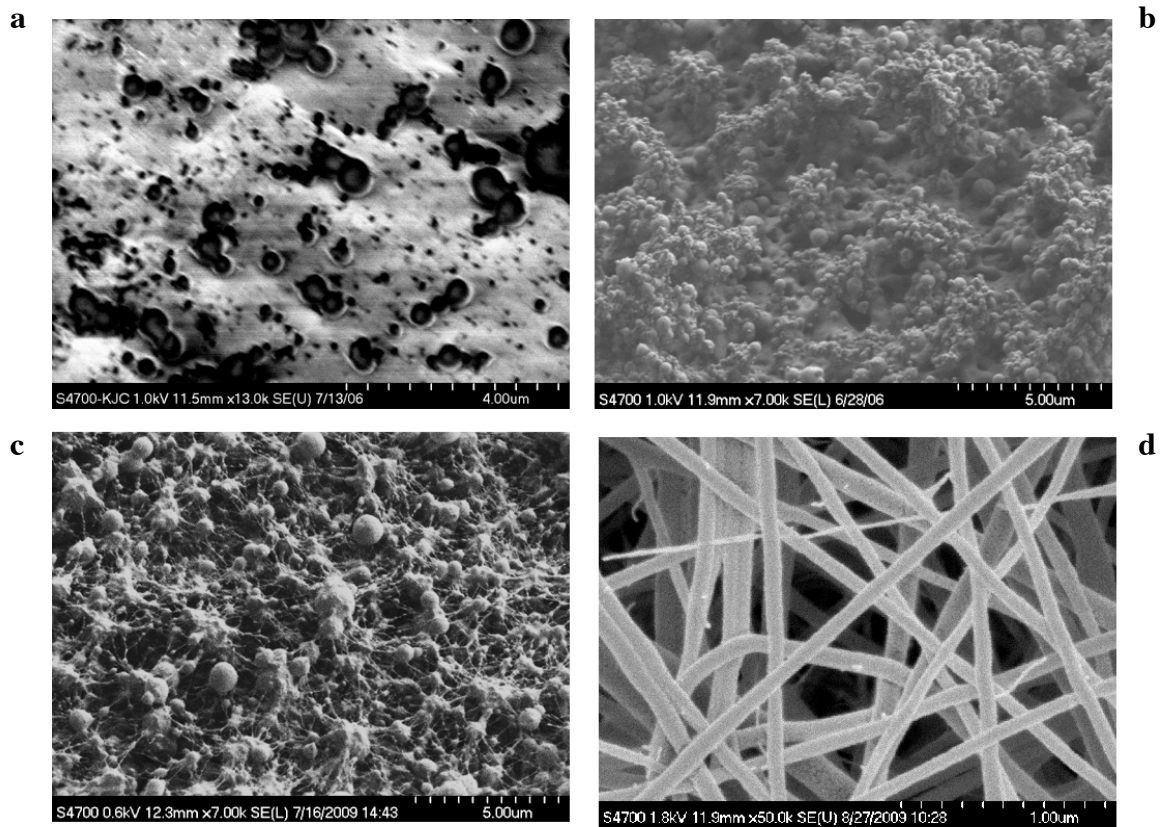


Figure 15. SEM images showing the effect of different electrospinning parameters. (a) polymer film produced by overly high syringe pump speed, (b) resolubilized protein blobs produced by insufficient electric field strength, (c) beads-on-a-string formed by low electric field strength, and (d) uniform fibres formed when electrospinning parameters are optimized.

Some short, very fine fibres were observed at the ends of broken fibres, and sometimes coming off of beads or fibres. An example of these fibres can be seen in the top left corner of Figure 15 d.

The parameters that produced the most uniform fibres (Figure 15 d) were 20 kV of electricity and 10 cm between source and collector, or 2 kV/cm. The syringe pump speed that produced the most uniform fibres was 0.02 ml/h. These parameters were used for all subsequent electrospinning of WECGP.

3.3 Polarized light microscopy

Isolated microfibrils teased directly from the egg capsules had a resting birefringence of 5×10^{-4} or greater (Didier, 2009). As expected, electrospun fibres from solubilized whelk egg capsule gland protein were also found to be birefringent (Figure 16), although less so than the microfibrils. Electrospun fibres immersed in oil to eliminate form birefringence were found to have an intrinsic birefringence of 6×10^{-6} or greater.

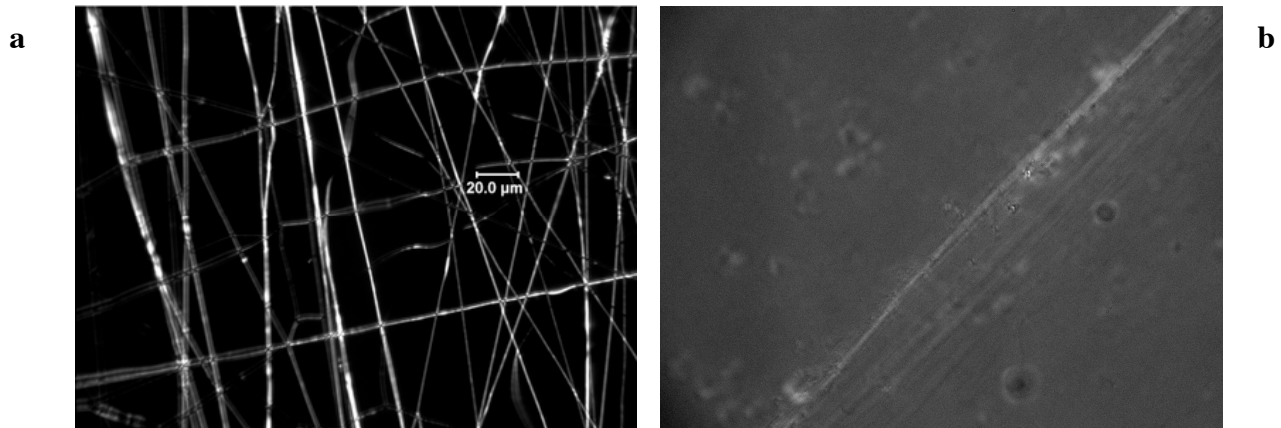


Figure 16. Polarized light microscopy images demonstrate that fibres electrospun from whelk egg capsule gland protein are birefringent, like fibres from the native egg capsule. Image (a) was taken in air and shows the total birefringence, which includes form birefringence. Image (b) was used to calculate the birefringence since the sample was in oil, which penetrates to give only the intrinsic birefringence of the electrospun fibres.

3.4 *The effect of PEO addition*

Poly(ethylene oxide) (PEO) was added to the WECGP solution in order to improve its processability. On its own, PEO formed nanofibres at concentrations of 5 wt% and 10 wt% in 88% formic acid (Figure 17, a-b). At 4 wt% in 88% formic acid, PEO formed fibres with the “beads on a string” morphology, and at 2 wt% and 3 wt%, PEO did not form nanofibres at all, only droplets (Figure 17, c-e).

2 wt% PEO was the proportion chosen for the WECGP electrospinning blend solution. This enhanced processability sufficiently for fibre formation although the PEO would be unable to form fibres on its own, indicating that PEO was not solely responsible for the production of fibres from the blend solutions.

Washing of samples to remove the PEO appeared to cause collapse of the fibre scaffolds, but the fibres themselves seemed to remain intact (Figure 18). Some breakage of fibres was observed, probably due to the scaffold collapse.

Because of its solubility in water, PEO had no effect on the mechanical testing of the electrospun fibres. Electrospun PEO test strips dissolved upon contact with the glue used to attach samples to the force transducer, and what remained of the samples pulled apart immediately. They appeared to lack any mechanical integrity and could not be tested. It is highly unlikely that they contribute anything to the mechanical properties of the fibres spun from the blend solutions.

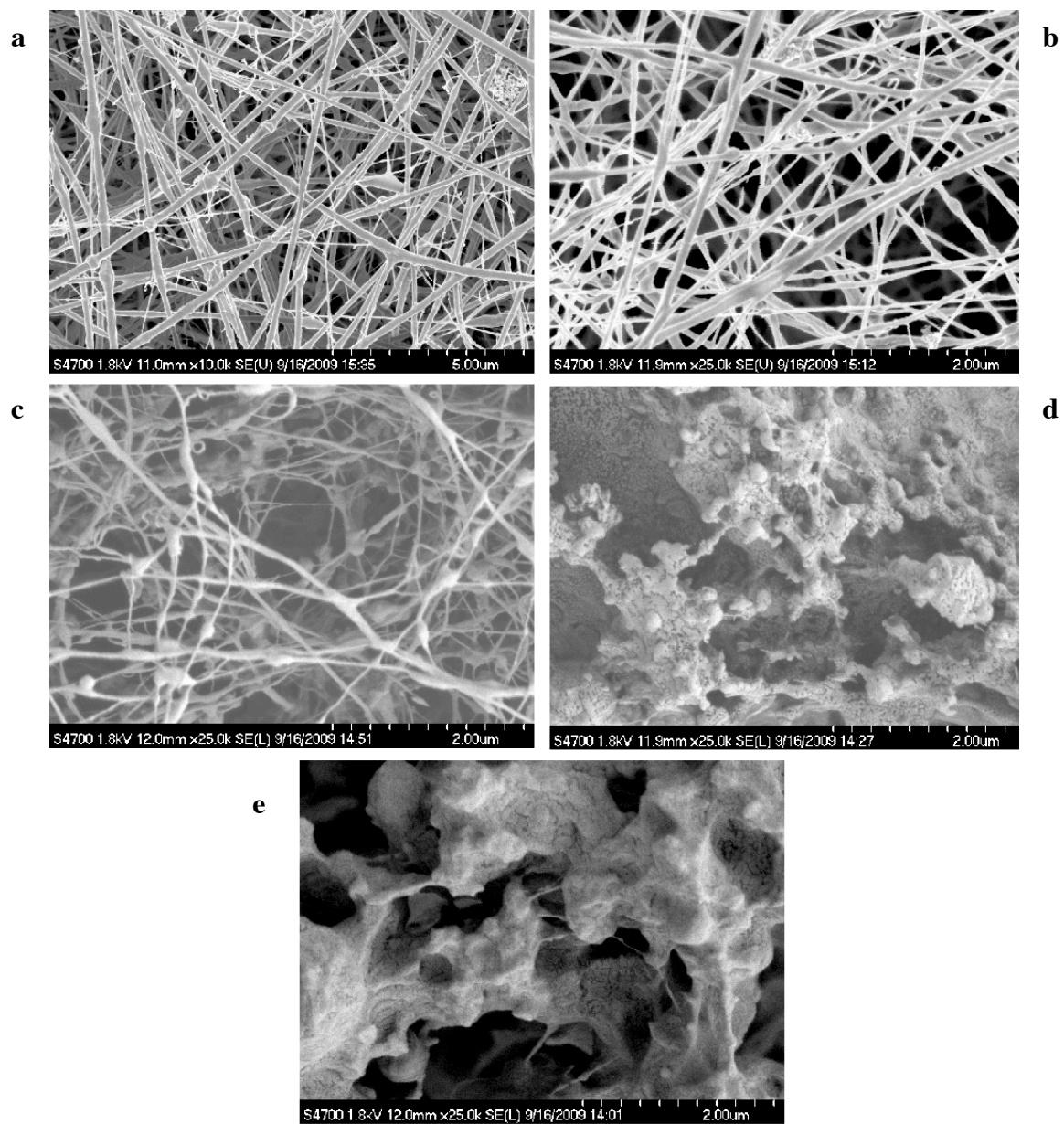


Figure 17. Scanning electron micrographs of Poly(ethylene oxide) (PEO) nanofibres. PEO was used to enhance fibre formation in the electrospinning WECGP blend solution. When electrospun on its own, PEO formed fibres at 10 wt% (a) and 5 wt% (b). At 4 wt% (c), PEO produced the “beads-on-a-string” morphology, and at 3 wt% (d) and 2 wt% (e) PEO failed to form fibres.

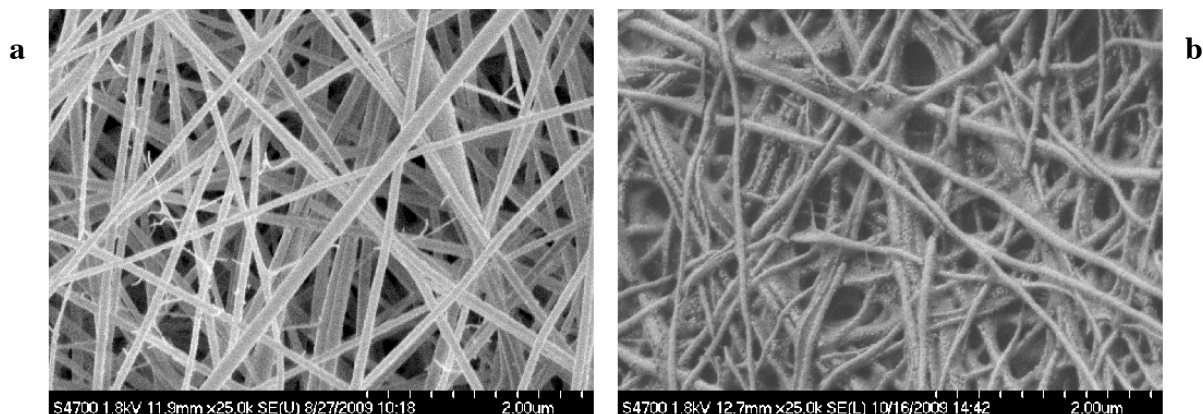


Figure 18. SEM micrographs of nanofibres electrospun from a blend solution of 8 wt% WECGP, 2 wt% PEO before (a) and after (b) washing with distilled water. Washing seemed to collapse the scaffold but did not appear to damage the fibres.

3.5 Measurement of electrospun fibres

With the overall polymeric concentration of the protein blend solutions held constant, the mean fibre diameter increased as the wt% PEO increased and the wt% WECGP decreased (Figure 19 a). The mean diameter increased from $0.0834 \mu\text{m}$ to $0.1731 \mu\text{m}$ as the wt% PEO increased from 2 to 5 wt%.

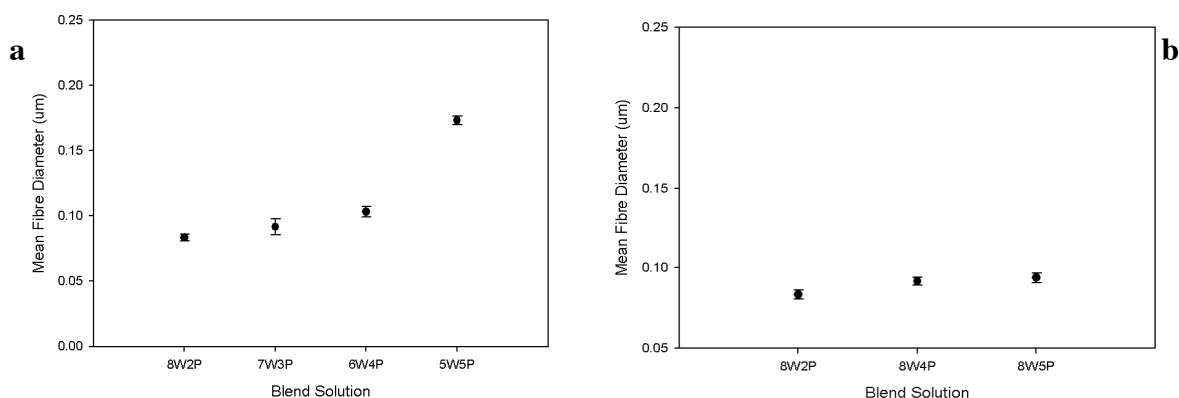


Figure 19. Mean diameters of electrospun fibres, \pm SE. Means were taken from a minimum of 100 individual fibre measurements. (a) constant total polymeric concentration, with wt% WECGP decreasing and wt% PEO increasing, (b) constant protein concentration, with wt% PEO increasing.

With the concentration of WECGP in the blend solutions held constant at 8 wt%, the average diameter of the fibres did not change significantly at 2, 4, or 5 wt% PEO (Figure 19 b).

Fibres electrospun from PEO alone increased in average diameter as the wt% PEO increased from 4 to 10 wt% (Figure 20). No fibres were produced at 2 or 3 wt% PEO. At 4 wt% the fibres had the undesirable beads-on-a-string morphology, which restricted the number of fibres available for diameter measurements. Therefore, the mean fibre diameter for the 4 wt% PEO solution is based on 40 individual fibre measurements, rather than the 100 measurements that comprised all other means.

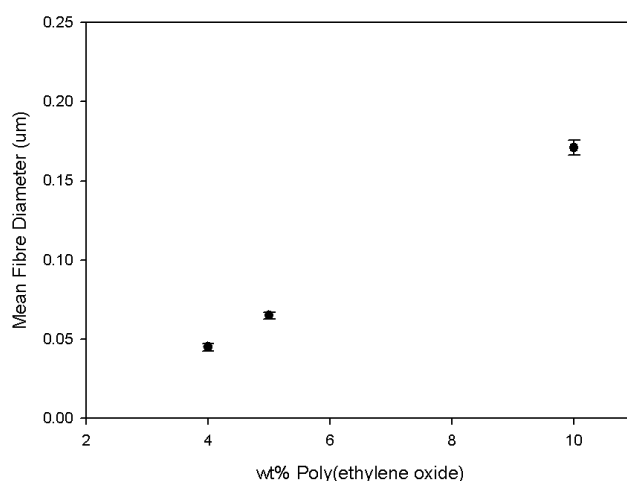


Figure 20. Mean diameters (\pm SE) of electrospun PEO fibres. Means were taken from a minimum of 40 individual measurements.

There were no similarities found in average fibre diameters of analogous solutions (Figure 21). At a total polymeric concentration of 10 wt%, the average diameter of PEO fibres was $0.171 \mu\text{m}$, more than double the average diameter of the 10 wt% protein blend fibres with the least PEO. Fibres produced from a 5 wt% PEO solution had an average diameter of $0.065 \mu\text{m}$, while fibres produced from a blend solution of 5 wt% protein and 5 wt% PEO had an average diameter of $0.173 \mu\text{m}$.

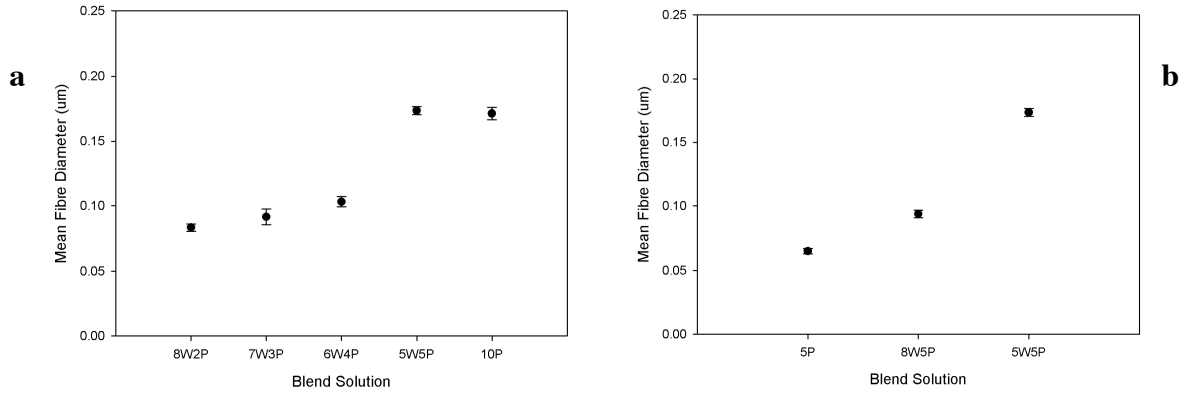


Figure 21. Mean diameters (\pm SE) of analogous solutions. (a) electrospinning solutions with a total polymeric concentration of 10 wt%, (b) electrospinning solutions that contained 5 wt% PEO.

The mean diameter of the washed fibres was $0.095 \mu\text{m}$ compared to a mean of $0.083 \mu\text{m}$ for the pre-washed fibres (Figure 22). This indicates that no material was lost from the fibres in washing with distilled water. Washing caused a collapse of the electrospun fibre scaffold, so the slight increase in average diameter may be due to a flattening of the fibres during the scaffold collapse.

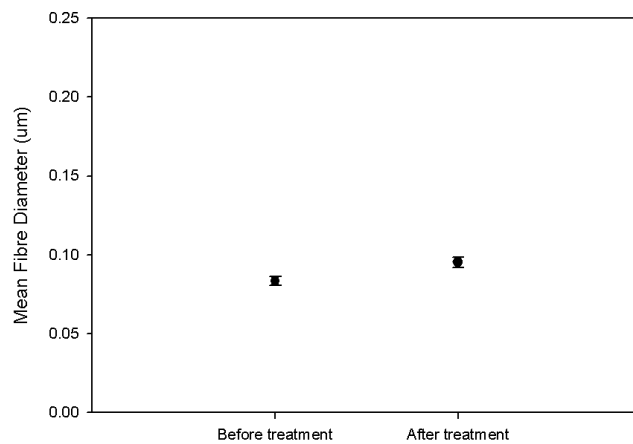


Figure 22. Mean diameters of fibres (\pm SE) electrospun from an 8wt% WECGP, 2wt% PEO solution, before and after washing with distilled water. Means were each calculated from 100 individual fibre diameter measurements. Unwashed samples were measured dry, and washed samples were dried under vacuum before measurement.

3.6 FTIR spectra

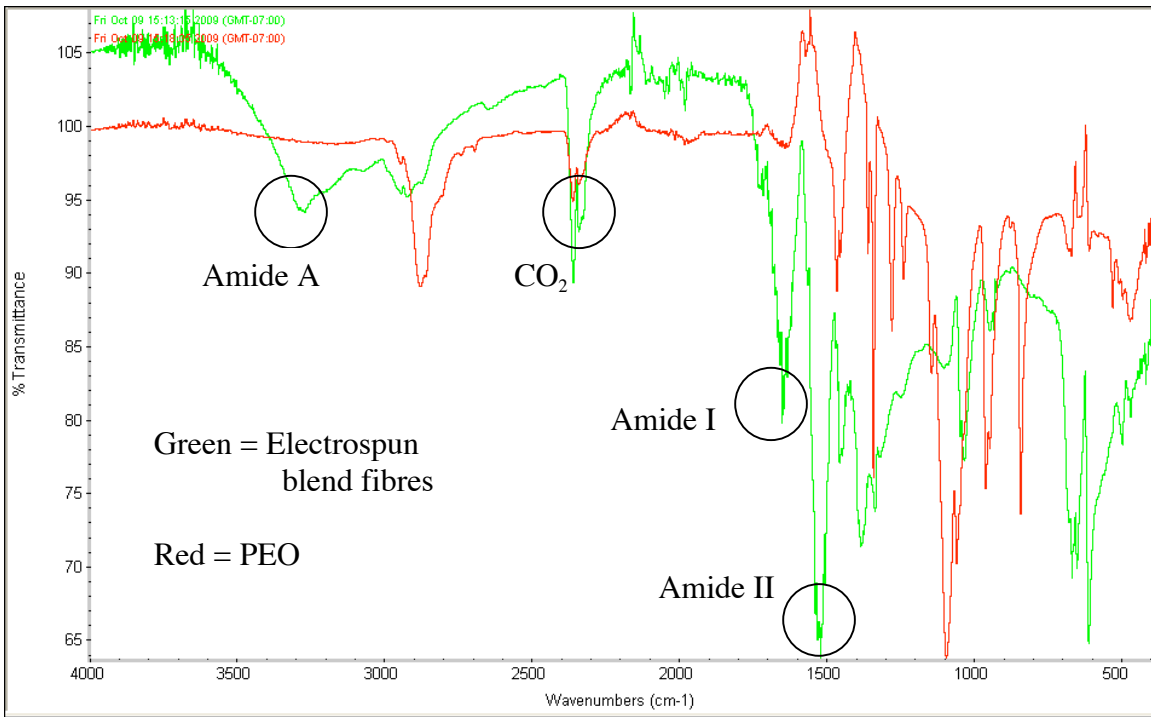
The FTIR spectra for PEO was overlaid on the spectra for electrospun fibres from the blend solution containing 8 wt% WECGP and 2 wt% PEO. The spectra for the freeze-dried WECGP was overlaid on the same electrospun blend fibre spectra. The spectra for the electrospun fibres was similar to that of the protein, and not similar to that of the PEO (refer to Figure 23).

The component curves of the amide I band for the freeze-dried WECGP and electrospun fibres were determined using a curve fitting procedure. In this way the contributions from peaks centred at the frequencies of well-characterized secondary structures were determined. Fortunately the amide I region of WECGP falls in a region that is not disturbed by PEO absorptions, so it can be used for structural study of the protein (Aluigi et al., 2008). Solvent interactions, which can affect the accuracy of the assigned frequencies for the component bands, do not need to be considered because solid samples were used.

Freeze-dried WECGP			Electrospun fibres		
Band position (cm ⁻¹)	Band assignments	% Content	Band position (cm ⁻¹)	Band assignments	% Content
1621-1640	β -Sheet	19	1621-1640	β -Sheet	18
1641-1647	Random coil	23	1641-1647	Random coil	22
1651-1657	α -Helix	21	1651-1657	α -Helix	21
1658-1671	Turns/bends	16	1658-1671	Turns/bends	17
1671-1679	β -Sheet	12	1671-1679	β -Sheet	13
1681-1696	Turns/bends	8	1681-1696	Turns/bends	9

Table 3. Composition of freeze-dried whelk egg capsule gland protein (WECGP) and electrospun fibres. Percents that do not add up to 100 are due to rounding.

a



b

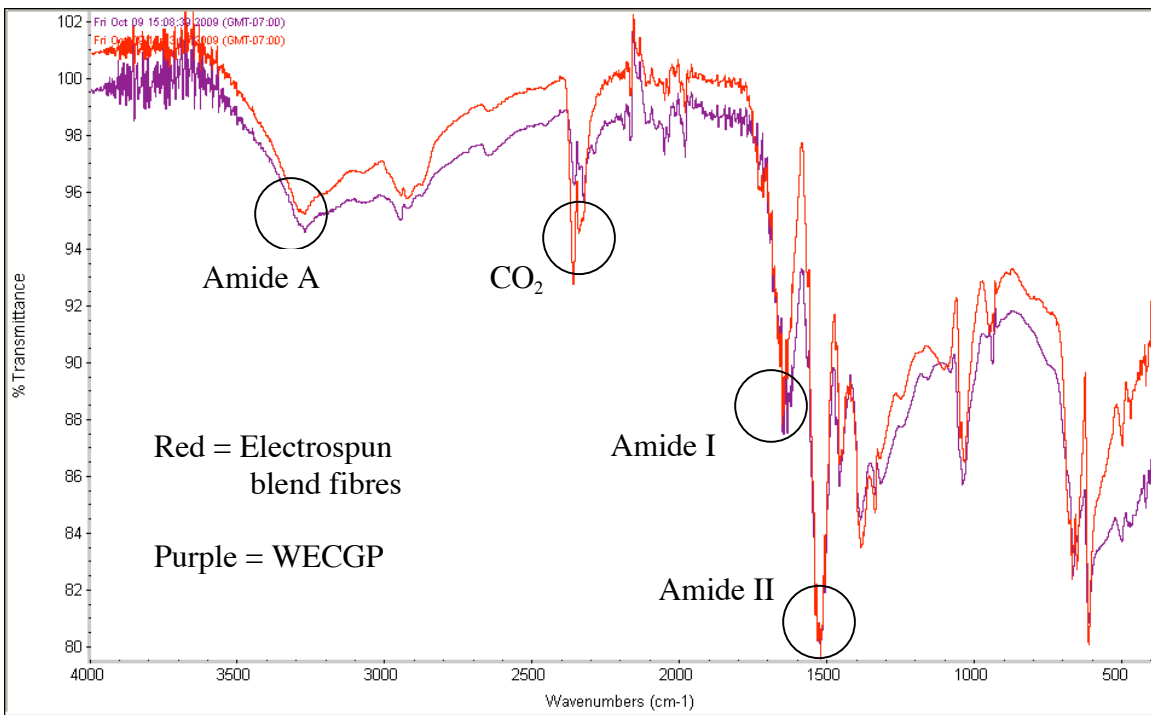


Figure 23. FTIR spectra (a) comparison of electrospun fibres from protein blend solution (green) to PEO (red), and (b) comparison of electrospun fibres from blend solution (red) to freeze-dried WECGP (purple). Differences in intensity between electrospun and protein spectra in (b) are within error.

3.7 Results of mechanical testing on electrospun fibres

Electrospun protein blend fibres were mounted on the testing apparatus and mechanically tested in one of three ways: 1.) as they were collected on the insect pins, 2.) after being cross-linked with glutaraldehyde, or 3.) draw-processed, cross-linked on the testing apparatus, and re-tested.

The electrospun fibres were white in colour, and became brownish-yellow if they were cross-linked. Samples that were not cross-linked would shear and slip during testing and did not return to their original length after testing. Draw-processed and then cross-linked samples were brittle and failed before 40% extension. Hysteresis data could not be collected for draw-processed samples as none of the samples survived the load cycle. Cross-linked samples did not slip and shear, or did so to a much lesser extent than uncross-linked samples (Figure 24). Neither the cross-linked nor the uncross-linked samples had stress-strain curves resembling those of the mature native protein, but the cross-linked samples appeared to be similar to the elastic transitional state in the maturation process of the capsule. The stiffly elastic Hookean region of the native protein was notably absent in the electrospun fibres.

The Young's modulus of the cross-linked electrospun fibres was 2.43, similar to that of the native capsule's yield region, where the modulus is 3.91 (Rapoport and Shadwick, 2002). Without being cross-linked, the electrospun fibres had a modulus of 0.15, an order of magnitude below the yield region of the capsule. The initial, stiffly elastic Hookean region of the capsule has a modulus of 87.9, 30X greater than the cross-linked electrospun fibres.

Hysteresis was calculated to be 0.51 and 0.69 for the cross-linked and uncross-linked electrospun fibres, respectively (Figure 25). Both of these hysteresis values are greater than the native capsule, indicating that more energy was lost and dissipated as heat during the loading and unloading cycle. Hysteresis loops did not change when a timed hold was inserted during extension.

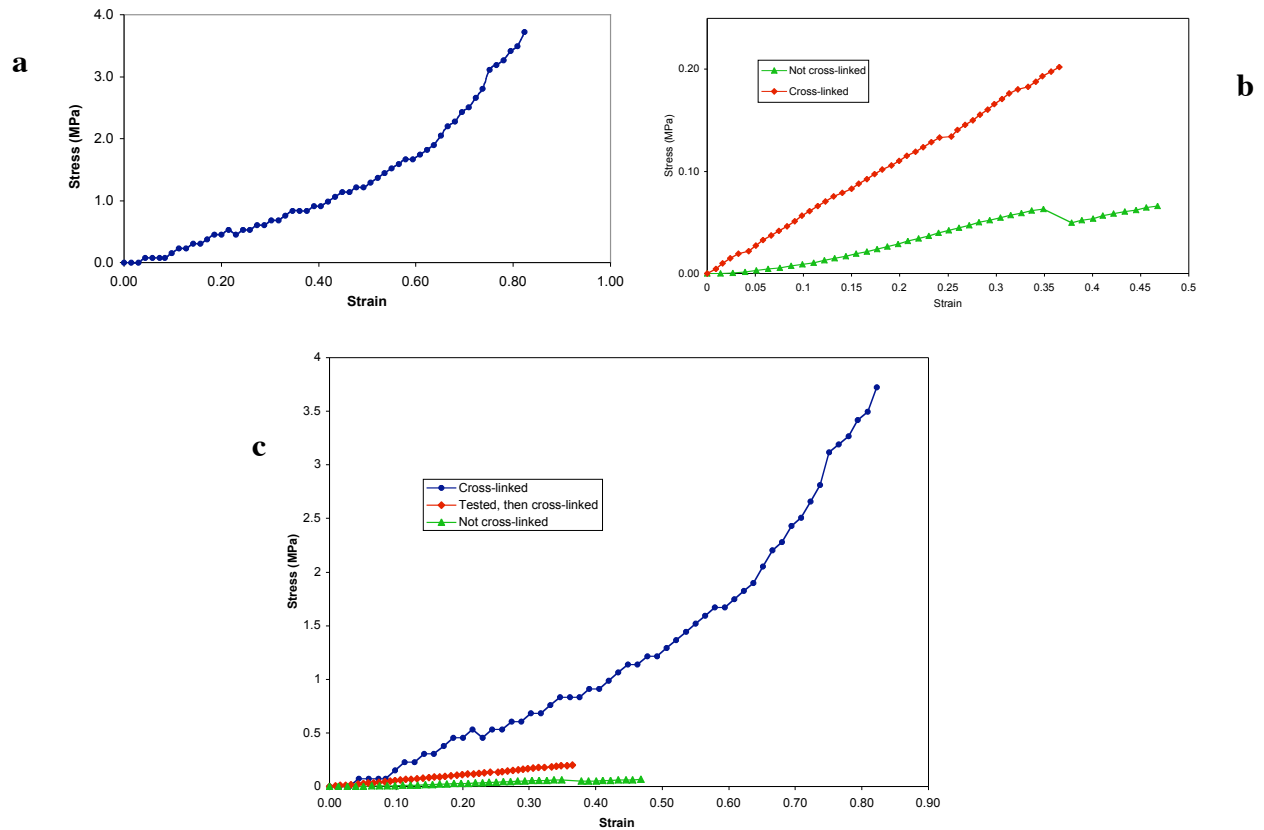


Figure 24. Stress-strain curves for electrospun WECGP samples. (a) cross-linked fibres, (b) fibres tested and then cross-linked after draw-processing. Before being cross-linked, the sample slipped at approximately 35% strain. (c) curves for cross-linked, draw-processed and then cross-linked, and uncross-linked fibres. Note different scales.

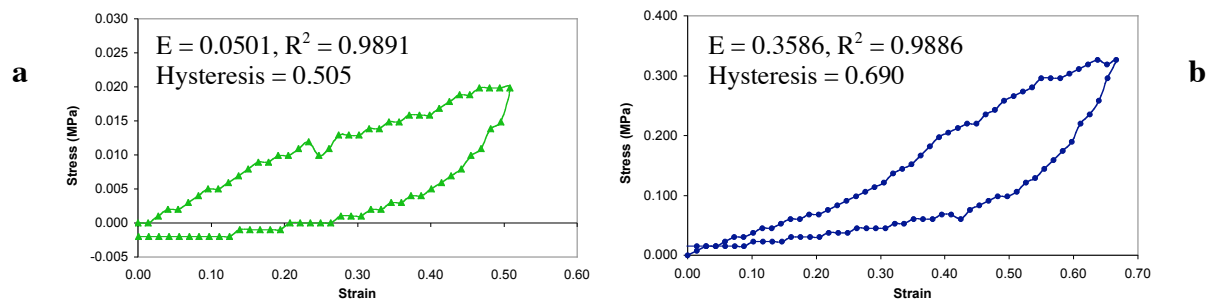


Figure 25. Hysteresis loops for (a) uncross-linked and (b) cross-linked electrospun WECGP protein blend fibres. Note difference in scales.

Material	Modulus (MPa)	Hysteresis
Not cross-linked	0.15	0.69
Draw-processed, then cross-linked	0.56	-
Cross-linked	2.43	0.51
Native capsule, Hookean region	87.9	0.20
Native capsule, yield region	3.91	0.37

Table 4. Young's modulus and hysteresis values for electrospun whelk egg capsule gland protein fibres, and for the native capsule. Capsule data from Rapoport and Shadwick, 2002.

4 Discussion

4.1 *Electrospinning parameters and the electrospinning of WECGP*

Samples of nanofibres have been produced in different conditions, but the optimal parameters for electrospinning the whelk egg capsule gland protein seem to be 1.) a distance of 10cm from needle tip to collecting target, 2.) an applied electric field of 20 kV, and 3.) a flow rate of 0.02 ml/hour, controlled by the syringe pump.

Increasing the distance between the needle tip and the target mandrel may allow for greater evaporation of the solvent but also decreases the strength of the electric field. If the distance is too short, the solvent will not fully evaporate and the jet will land on the target still wet, forming globular droplets rather than fibres. This can be ameliorated by lowering the ambient humidity or by choosing a solvent with a larger difference between its vapour pressure and that of air (Yang et al., 2006). If ambient humidity is low, increasing the distance between source and target will result in lower fibre diameters as more solvent evaporates, but if ambient humidity is high, there will be no increase in solvent evaporation (Yang et al., 2006). No attempts were made to adjust the ambient humidity during the course of this study since formic acid proved volatile enough to evaporate appropriately.

On the other hand, if the vapour rate of the solvent is too fast, the fibre diameter will increase (Yamashita et al., 2007). There are also other techniques to remove unwanted solvent residue. Spasova et al. (2007) placed electrospun samples under vacuum to remove solvent residue in order to improve conditions for cell growth on their electrospun fibre scaffolds.

In this study, short distances between needle tip and target produced either a protein film or globular protein deposits on the collecting foil, but no fibres. The film was due to resolubilization of the protein on the target, caused by incomplete evaporation of the

solvent. Globular protein deposits were likely due to clumping at the needle tip, which was caused by inadequate electric field strength. Increasing the electric field strength at short distances produced a spark between the charged needle and grounded target. At distances of less than 5 cm between needle and target, a spark was discharged when the electric field was applied, even at low electric field strength. This indicates breakdown of the electric field.

At distances between source and target of greater than 15 cm, fibres were no longer reliably deposited on the collector. The amplitude of the whipping motion of the electrified polymer jet increases with distance from the needle, making it less likely that nanofibres will be collected in a small area. Working with PEO, Yang et al. (2006) found that short distances between source and target prevented fibre formation, and long distances resulted in a larger distribution of fibre diameters. Electric field strengths greater than 30 kV also increased the amplitude of the whipping motion, and caused the polymer jet to fluctuate wildly. This also led to poor deposition of nanofibres on the collector, and an impressive mess within the electrospinning chamber.

In their topical review of electrospinning design, Teo and Ramakrishna (2006) summarized the advantages and disadvantages of the rotating mandrel as a means of collecting electrospun fibres. The advantages were the simplicity of the set-up and the ability to collect large areas of fibres, but the drawback was that highly aligned fibres are difficult to fabricate, as observed in this study (Teo and Ramakrishna, 2006). The mandrel of the Kato Tech NEU-010 was not able to rotate quickly enough to produce aligned nanofibres of WECGP. The mandrel was also so large (8 cm diameter) that when it was rotating, very low fibre density was produced even when electrospinning for many hours. This was not helped by the slow flow rate (0.02 ml/h) used to produce WECGP nanofibres.

Teo and Ramakrishna's (2006) review of another electrospinning set-up involving a pair of parallel electrodes sparked the idea for the paired insect pins used in this study to collect samples for mechanical testing. They found that using parallel electrodes as a

collecting device made highly aligned fibres easy to obtain, and that the aligned fibres were easily transferable to another substrate (Teo and Ramakrishna, 2006). The paired insect pins were mounted parallel to each other and perpendicular to the target mandrel, pointed at the source needle. The pins were mounted beneath the aluminum foil that covered the target mandrel and emerged by piercing the foil, effectively increasing the available surface area of the grounded target. Electrospun fibres that spanned the gap between the pins could be transferred for use in mechanical testing with minimal handling. Upon visual inspection, these fibres showed a marked increase in alignment compared to fibres deposited directly onto foil, probably because fibres of different orientations failed to span the gap between the pins and thus were deposited elsewhere.

Several unsuccessful attempts were made over the course of this study to electrospin WECGP nanofibres directly onto glass. Li et al. (2005) electrospun protein fibres onto cover glasses that were attached to a brass grounded target. In this study, however, fibres were not convinced to land on a glass target, whether it was attached to a grounded target, covered in foil with only a small window of glass exposed, or even if the glass was sputter-coated with gold before being attached to the grounded target.

In an attempt to eliminate handling of samples prior to mechanical testing, a small force transducer was made using an 80 nm glass rod and a cover slip attached to a micrometer, which slid on a drop of vacuum grease. These were mounted onto a microscope slide and sputter-coated, first with 8 nm of gold, then with a further 8 nm. The entire apparatus was grounded, but the fibres stubbornly refused to span the gap between the rod and cover slip.

Two distinct size groupings of nanofibres were often observed on the SEM images. The main group was composed of uniform fibres, which were measured to determine the average diameters of the blend solutions. The second group was at least an order of magnitude smaller in diameter, was generally short in length, and tended to emerge from main group fibres and beads. These fibres were less stable when viewed under the SEM and would quickly melt and curl under the electron beam. Yang et al. (2006) proposed

that short, very fine fibres observed at the ends of broken fibres, or seen coming off of beads and other fibres may be caused by strong electrical forces on fibres with little remaining solvent.

The egg capsule gland has been used in this study as a source of protein for electrospinning because it is composed of the precursor protein. The precursor protein has not been mechanically manipulated or cross-linked by the whelk, so it is more soluble than the mature capsule. However, “soluble” here is a relative term. The gland protein was solubilized using a mortar and pestle, brute force, and blood, sweat, and tears in 88% formic acid. Formic acid was chosen for its ability to solubilize the protein, its volatility, and because it vapourizes without leaving a residue. This protein does not solubilize without strong coercion, and even so would not solubilize in formic acid to the critical concentration required for electrospinning.

In dilute solutions, polymers form separate hydrated coils that do not interact with each other. As the polymeric concentration of the solution increases, the coils go from moving independently to overlapping and becoming an entangled network. These polymeric interactions are necessary for the electrospinning of continuous fibres, therefore the electrospinning solution must have a critical concentration of polymer.

Tris 2-carboxyethyl phosphine (TCEP) was added to the formic acid to enable the egg capsule gland protein to reach the critical concentration for electrospinning. TCEP acts as a reducing agent to break disulfide bonds in the protein, thus decreasing the viscosity of the solution. TCEP was selected because it is able to reduce these bonds at lower pH than dithiothreitol (DTT), and it smells much better than mercaptoethanol. 25 mM was found to be sufficient to break the protein into its 50 kDa monomeric subunit.

4.2 PEO

Poly(ethylene oxide) (PEO) is added to the electrospinning solution to increase the viscosity, improve processability, and encourage fibre formation. Nanofibre-producing solutions of the whelk egg capsule gland protein used for this study consisted of 8 wt% protein, 2 wt% PEO, and 25 mM TCEP solubilized in 88% formic acid.

The change in morphology from beads-on-a-string to continuous nanofibres, which was observed with increasing amounts of PEO, is likely the result of the increase in solution viscosity (Aluigi et al., 2008). On its own, PEO formed nanofibres at concentrations of 5 wt% and 10 wt%, formed fibres with the “beads on a string” morphology at 4 wt% and did not form nanofibres at all at 2 wt% and 3 wt%. The lower viscosities of the latter solutions do not allow sufficient molecular chain entanglements to prevent breakage of the electrically driven jet formed by the electrospinning process (Aluigi et al., 2008). The fact that PEO did not form fibres at 2 wt% unless WECGP was also present indicates that WECGP is the primary component of the fibres electrospun from the blend solution, and that PEO was playing a supporting role.

Aluigi et al. (2008) found that nanofibres rich in protein were more homogenous than nanofibres rich in PEO. This indicates that the blend composition plays an important role in determining the diameter distribution of the fibres and was one of the reasons the amount of PEO in the blend solution was minimized. Since the PEO solution series often did not form fibres, or formed only very few, in a “beads on a string” conformation, it is difficult to draw conclusions about whether these fibres were more or less homogenous than the fibres spun from the protein blend solution. In addition, only 40 fibre diameters per PEO solution were measured, compared to 100 for each of the protein blend solutions, which makes the standard error of the means less comparable.

4.3 Nanofibre diameter

The diameter of electrospun fibres is influenced by many factors, such as protein concentration, viscosity, field strength, distance between polymer source and target, and flow rate. In this study a distance of 10 cm between the needle tip and the target mandrel was used, with an applied electric field of 20 kV. The electrospinning voltage was 2 kV/cm, past the upper limit determined by Katti et al. (2007) that produces the smallest diameter fibres.

As expected, the average diameter of WECGP blend nanofibres decreased as the protein concentration increased. Aluigi et al. (2008), looking at the effect of protein concentration, found that as the keratin content of their electrospinning solution increased, the average nanofibre diameter decreased. They also found that the diameter distribution was narrower in keratin-rich nanofibres (Aluigi et al., 2008). This may be due to several factors, including changes in the viscosity and conductivity of the solution. When a higher charge density is carried by the polymer jet, it forms smoother, finer nanofibres because it produces stronger whipping instability, which enhances filament stretching (Aluigi et al., 2008). Lower viscosity has also been shown to promote the formation of smaller diameter nanofibres (Aluigi et al., 2008).

In this study, when the protein concentration was held constant, the amount of PEO in the polymer blend solution did not significantly change the average diameter of the fibres. This suggests that once the protein component of the blend solution reaches some critical concentration, the protein controls the fibre diameter.

Li et al. (2005), found that increasing the syringe pump flow rate from 1 to 3 ml/h caused a significant increase in fibre diameter for both collagen and gelatin, although a further increase from 3 to 8 ml/h did not significantly affect the mean diameter. In this study, the syringe pump flow rate that produced the smallest, most uniform fibres was 0.02 ml/h. Flow rates of this order of magnitude have successfully produced electrospun fibres from many different polymer solutions, but increasing flow rates to scale up

production has been key for many applications, so a slow flow rate has not been considered desirable. However, WECGP blend solutions did not produce fibres until the flow rates from the literature had been decreased a hundredfold.

When determining the average diameter of the electrospun fibres from the SEM micrographs, it was not possible to distinguish if one fibre was measured more than once. Fibres are laid down on the collector in a looping deposition pattern, so a single fibre may cross the image field of view repeatedly and thus be measured repeatedly. However, considering the vast number of fibres deposited in a spinning session, this was assumed to be a rare occurrence that would not have greatly skewed an average of 100 measurements.

4.4 Birefringence of electrospun fibres

Fibres electrospun from the protein blend solution (8 wt% protein, 2 wt% PEO, and 25 mM TCEP solubilized in 88% formic acid) were found to be birefringent, which indicates that the fibres have an ordered structure. Since the process of electrospinning aligns molecules on the basis of charge, and induces the formation of fibres based on this alignment, it is not surprising that they have ordered structures. Birefringence scans of whelk egg capsules showed that the native material is highly birefringent (Rapoport and Shadwick, 2007), and further work by Didier (2009) demonstrated that individual protein fibres teased out of the native capsule are also birefringent.

Birefringence tends to increase as a material is strained, and Didier (2009) found that this is true for individual fibres of the whelk egg capsule, but only in the Hookean region. After the transition to the yield region the birefringence decreases, indicating a loss of overall order in the structure as α -helices are pulled apart (Didier, 2009). The FTIR data on the electrospun fibres showed that the fibres had 21% α -helical character, same as the purified WECGP, so it is possible that the α -helices were also being pulled apart when the cross-linked electrospun fibres were strained.

The samples of electrospun fibres used to measure birefringence contained as few fibres as possible given the collection method. Even so, the diameters of the samples were between 1.0 and 1.5 μm . Since we know that the individual electrospun fibres are only about 100 nm in diameter, each sample measured must have been composed of many smaller fibres. It is difficult to resolve detail on a fibre that is less wide than a wavelength of light.

4.5 The Matrix Squeeze hypothesis

Applying part of Fudge and Gosline's "matrix squeeze" hypothesis for intermediate filaments (IFs) (2004), which argues that the matrix restricts the hydration of IFs, thus regulating water's role as a plasticizer, we would expect WECP to exhibit lower stiffness and strength when hydrated. WECP acts as predicted by this hypothesis – it is hydrated in its native state, and becomes stiffer and stronger when dehydrated, with both its yield stress and initial modulus increasing by an order of magnitude (Rapoport and Shadwick, 2007). Hydration did not seem to have an effect on yield strain (Rapoport and Shadwick, 2007).

Cross-links are thought to restrict the hydration of IFs, allowing H-bonding to dominate, increasing modulus and yield stress (Fudge and Gosline, 2004). Matrix-free IFs such as hagfish slime threads are very hydration sensitive and swell greatly as they hydrate, but matrix acts to restrict hydration of IFs by resisting deformation (Fudge and Gosline, 2004). An elastomeric matrix that resists circumferential expansion such as hydration swelling will also resist longitudinal deformation from applied tensile forces and improve IF recovery (Fudge and Gosline, 2004).

Drying WECP seems to make it more similar to hydrated α -keratin, but because cross-link (or matrix) density in WECP is lower than keratin, WECP does not attain a modulus as great as keratin (Rapoport and Shadwick, 2007). This difference in cross-link density is probably due to both the environment in which the materials are expected to operate

and their adaptive functions (Rapoport and Shadwick, 2007). Stiffer keratins such as hoof, hair, and horn do not need to be diffusive barriers, while whelk embryonic development may be compromised by a more cross-linked and therefore less diffusive capsule (Rapoport and Shadwick, 2007).

The cross-linking agent used in this study was glutaraldehyde, which tends to quickly form many, fairly indiscriminate cross-links. The density of cross-links was not controlled, although it is likely that the native protein has a much more specific cross-linking strategy. However, even with this uncontrolled cross-linking, the electrospun fibres did not attain the stiffness or strength of the mature egg capsule.

4.6 Self-assembly of elastic polymers

Research has so far not been able to find one obvious protein sequence that gives elastomers their elastic recoil properties (Keeley et al., 2002). The way monomers are organized into polymeric structures must be crucial for elastomeric properties (Keeley et al., 2002). Elastin, for example, is synthesized as a monomer, assembled in the extracellular matrix, and stabilized by covalent cross-links derived from side chain lysine residues (Keeley et al., 2002). The monomer has a strong tendency for self-aggregation, and this intrinsic ability to self-assemble is seen even in relatively small recombinant peptides based on human elastin sequences (Bellingham et al., 2003).

Keeley et al. found (2002) that the process of self-assembly aligned the elastin monomers such that cross-linking of lysine residues could take place. They showed that small numbers of hydrophobic and cross-linking domains could provide this ability for self-alignment and impart the properties of extensibility and elastic recoil (Keeley et al., 2002). Bellingham et al. (2003) demonstrated that as few as three hydrophobic domains flanking two cross-linking domains in recombinant peptides are sufficient to support a self-assembly process that aligns lysines and forms the cross-links of native elastin. They also showed that these cross-linked polymers have physical and mechanical properties

similar to native elastin (Bellingham et al., 2003). It is likely that the self-assembly process of WECGP similarly aligns monomers such that cross-linking can take place, albeit with the assistance of a muscular massage in the ventral pedal gland. It is possible that a chemical change takes place at the VPG, but this has been neither confirmed nor ruled out.

4.7 Using FTIR to positively identify WECGP in electrospun fibres

The FTIR spectra for freeze-dried WECGP and a sample of fibres electrospun from a blend of 8 wt% WECGP, 2 wt% PEO and 25 mM TCEP in 88% formic acid were nearly identical, indicating that WECGP was in fact the dominant component in the fibres. The slight shift in intensity was within experimental error. Three absorbance peaks characteristic of proteins were strongly mirrored in the two spectra, at amide A, amide I, and amide II. The largest difference between the spectra was the absorbance peak at 2350 cm^{-1} , which is an artifact of atmospheric CO_2 .

PEO is a synthetic polymeric material that is well known for its “spin-ability”. Since PEO is so keen to form fibres by electrospinning, it was a useful addition to the protein blend solution, but simply electrospinning PEO was not the purpose of this study. Qualitative tests of electrospun fibres formed from the blend solution (8 wt% WECGP, 2 wt% PEO, 25 mM TCEP in 88% formic acid) had indicated that the fibres were indeed protein. For example, the fibres were not water soluble, and PEO dissolves instantly in water. However, stronger evidence was desired. Therefore, the FTIR spectra for PEO was compared to the spectra for the sample electrospun from the blend solution. The two spectra showed a similar absorbance peak at 2350 cm^{-1} , the artifact peak for CO_2 , but had very little similarity otherwise. Not surprisingly, PEO lacked the amide absorbance peaks characteristic of proteins, which were the dominant peaks in the electrospun fibres’ spectrum. The first large absorbance peak on the PEO spectrum was at 3150 cm^{-1} , which is not a frequency of interest for proteins.

4.8 *Determining secondary structural changes using FTIR*

The FTIR spectra of any protein will consist of three types of amide bands, at characteristic frequencies. The bands represent the bonds between the amide, alpha carbon, and carbonyl groups that make up the basic structure of all amino acids. Amide I is the most intense absorption band in proteins. It is found between 1600 cm^{-1} and 1700 cm^{-1} , and is primarily due to stretching of the C=O bond in the carbonyl group. Amide II is found between 1520 cm^{-1} and 1540 cm^{-1} , and represents deformation of the N-H bond in the amide group. Amide III is found between 1230 cm^{-1} and 1270 cm^{-1} , and results from bending of the C-N bond between the amide and the alpha carbon. The frequencies of these amide bands can be used to determine the secondary structure of proteins. The amide I band of WECGP is not disturbed by the PEO absorption spectra. Therefore, it can be used cleanly to study the structure of WECGP in the nanofibres.

Different protein conformations show different FTIR absorption bands. α -helices show strong absorbance in the amide I band between 1651 and 1657 cm^{-1} . β -sheets show strong absorbance in the amide I band between 1621 and 1640 cm^{-1} , and between 1671 and 1679 cm^{-1} . Using the amide I band for calculations, the ratio of the area under these intervals to the total area under the amide I curve will give the percentage of α -helix or β -sheet in the sample, respectively.

The calculated % α -helix in the electrospun sample was 21% and the calculated % β -sheet was 32%. The calculated % α -helix in the freeze-dried WECGP sample was also 21% and the calculated % β -sheet was 31%. From these results it appears that β structures are more prevalent in the protein than helical structures, which is contrary to the model proposed by Rapoport and Shadwick (2007) and supported by Didier (2009) and Miserez et al. (2009). However, these results are for the immature protein, and the model is for the mature capsule.

Protein	Collagen	Elastin	Keratin	WECGP
% α -helix	19	24	42	21
% β -sheet	28	41	19	31

Table 5. Secondary structure composition in common structural proteins and WECGP. All data is from FTIR studies. Collagen was type I, from bovine skeletal muscle tissue – note that in addition to 19 % α -helix there was an additional 18 % triple helix (Petibois et al., 2006). Elastin was from human aortic tissue (Bonnier et al., 2008), and keratin was from horsehair (Kreplak et al., 2004).

Although we have evidence that the α -helices of the native protein are pulled apart when the egg capsule is strained, it seems that the β -sheets that form as a result of the strain are not stable (Didier, 2009). The protein does not irreversibly pull apart; rather, its α -helices rapidly reform once strain is removed, even generating force while doing so (Didier, 2009). This is interesting since the α -helix to β -sheet transformation is often irreversible since the β -sheet structure forms a new stable state. It would be interesting to use FTIR to obtain spectra of both the mature protein and electrospun fibres, held at different extensions to look more closely at how the secondary structures are affected by strain.

Looking at FTIR results analyzing the secondary structure of other structural proteins, we see that keratin has the most α -helix (42%), followed by elastin at 24%, and collagen at 19%. Keratin, which is very stiff, would be expected to have a high proportion of α -helix, but the collagen data is mysterious since collagen is almost entirely triple helix. The FTIR data from Petibois et al. (2006) indicates that only 18% of the secondary structure of collagen is triple helix, and that it is 19% α -helix and 28% β -sheet. There must be an interesting explanation. From the FTIR data, WECGP is unexpectedly closer in α -helical character to elastin than keratin. This may be related to the fact that the electrospun fibres, even when cross-linked, did not reproduce the stiff Hookean region of the mature protein, but only the rubbery yield region. The Hookean region is attributed to α -helices, and develops last in the native protein's maturation sequence.

4.9 *Cross-linking of electrospun fibres*

Electrospun fibre scaffolds from the blend solutions lack the strength of the mature native protein and were therefore treated to improve their mechanical integrity. Cross-linking can be used to tailor biomechanical characteristics to match that of the original material, in this case WECGP. It does not appear that the native cross-links form to any significant degree, if at all, in the electrospun fibres.

Glutaraldehyde, as a cross-linking agent, has many advantages. It is relatively inexpensive, cross-links over varying distances, reacts quickly, and reacts with many amino groups present in proteins (Barnes et al., 2007). Glutaraldehyde reacts mainly with primary amines in proteins (Barnes et al., 2007). Although glutaraldehyde is the most popular agent for cross-linking biological materials, it is known to be cytotoxic and to compromise biocompatibility (Barnes et al., 2007).

Interestingly, Buttafoco et al. (2006) found that the cross-linking process resulted in the leaching of PEO from fibres originally electrospun from 1:1 by weight type I collagen and PEO. They also observed that the fibre morphology was not modified after cross-linking (Buttafoco et al., 2006).

Both glutaraldehyde and carbodiimide have been used for cross-linking electrospun mats produced from type II collagen. Unlike fibres produced by electrospinning WECGP, type II collagen fibres disintegrate upon contact with aqueous solutions, making the cross-linking process more difficult if the nanofibrous morphology was to be conserved (Barnes et al., 2007). Aluigi et al. (2008) had similar difficulties with electrospun keratin nanofibres – they were also water soluble and had poor mechanical properties since they were not cross-linked. Mechanical properties of cross-linked collagen mats were measured in the hydrated state, as were the WECGP mats in this study, to show behaviour under approximate physiological conditions.

Barnes et al. (2007) found that the stress-strain curves of cross-linked collagen fibres behaved more like native collagen than untreated samples. In collagenous structures there is a non-linear toe region in which the collagen fibres align, then the aligned collagen fibres are collectively stretched. The non-woven electrospun mats appeared to follow the same procedure during extension, with the electrospun fibres aligning in a toe region, then being collectively stretched (Barnes et al., 2007). Barnes et al. (2007) reported that the stiffness of the electrospun mat depends upon fibre diameter, orientation, and number of fibres, as well as the strength of the covalent cross-links and the type and amount of non-covalent bonds.

4.10 Mechanical testing of electrospun fibres

The simplest method, and the model proposed by Altman et al. (2002) assumes that a bundle of multiple fibres acts as a single fibre with an effective radius determined by the number and radii of the individual fibres. This model ignores friction between the individual fibres, and assumes parallel alignment of the fibres (Altman et al., 2002). However, the silk fibres produced in the very cool study by Altman et al. (2002) were orders of magnitude larger than those produced in this study, and the silk fibres were highly controlled for alignment using a clever hierarchical approach.

Due to the variable orientation of electrospun fibre deposition in this study, even with the greater alignment inherent in the insect pin spanning structure, the samples used for mechanical testing were not uniform. However, the estimation of sample thickness used to calculate the cross-sectional area should not have contributed too much error to the stress values. Samples were assumed to be rectangular, and the width was measurable. Assuming a circular cross-section would have created more error, since the estimated value for the radius would have been squared, compounding the effect of the estimate. However, the samples were measured hydrated, immediately before they were tested. Hydration is likely to have caused the sample to swell, especially given the very low density of the fibres in each sample. Therefore, the cross-sectional area measurements

will all have been overestimated, which results in all the stress values being underestimated. It is not unreasonable to think the actual values could be double what was measured in this study.

The addition of synthetic polymers to electrospinning solutions is common and has been shown to affect the mechanical properties of the resulting fibres. Jeong et al. (2007) electrospun a synthetic polymer onto the surface of tissue-engineered collagen scaffolds to improve their mechanical strength. The synthetic polymer, PLGA, was found to increase the scaffold strength in both the wet and dry states (Jeong et al., 2007). PEO, on the other hand, could not have affected the mechanical strength of the electrospun fibres in this study since PEO is water soluble, and all samples were mechanically tested in aqueous conditions. When an attempt was made to test the mechanical strength of a mat of PEO fibres, the mat disintegrated upon contact with the glue, and so could not be tested. Therefore any remnant of PEO that did not immediately dissolve when placed in the water chamber would dissolve upon contact with the glue, and without being glued to the strain gauge the PEO would be unable to contribute to the force measurements.

4.11 Mechanical results

The native protein of the whelk egg capsule undergoes a maturation process, with different characteristic stress-strain curves for different steps of the process. If the protein is mechanically tested early in the process, before the capsule is manipulated by the ventral pedal gland, the protein lacks mechanical integrity (Rapoport and Shadwick, 2007). At this point the protein is thought to have self-assembled but not yet cross-linked. The native protein then undergoes a muscular massage in the VPG, where it is thought that layers of the protein are brought close together, enabling crosslinking, or where some chemical change may occur. This produces an elastic, cross-linked, transitional state before the capsule is fully mature. The electrospun protein fibres appear to be similar to the native protein in this transitional stage.

The cross-linked electrospun fibres did not yield stress-strain curves similar to the mature native protein. The electrospinning process aligns and assembles the solubilized protein monomers according to charge, and the current maturation model starts with charge-based self-assembly of microfibrils (Rapoport and Shadwick, 2007). However, there may be a much more specific process during self-assembly that produces the correct locations and number of locations for cross-linking later in the maturation process.

The Young's modulus of the cross-linked electrospun fibres was the same order of magnitude as the yield region of the mature capsule, but still an order of magnitude below the modulus of the egg capsule's stiffly elastic Hookean region. Without being cross-linked, the electrospun fibres had a modulus an order of magnitude below even the yield region of the capsule.

The electrospun fibres were cross-linked with glutaraldehyde, rather than by a mysterious muscular massage. Glutaraldehyde is likely not as specific, seeing as it reacts with many different amino groups, and it reacts over various distances, which is unlikely to be the case for the native protein, or the massaging should not be necessary. The cross-linked electrospun samples lacked the Hookean region of the stress-strain curves of the mature protein. This region is the last to form in the maturation timeline of the protein, and it signals that the material properties are fully developed.

All of the cross-linked electrospun collagen structures produced by Barnes et al. (2007) had values of modulus and peak stress at least one order of magnitude less than those reported for the native cartilage tissue that the collagen was derived from, and the breaking strains of the electrospun mats were greater than that of the native cartilage. The breaking stress of cross-linked electrospun samples in this study was an order of magnitude less than the native protein. The breaking strains were the same order of magnitude, although the electrospun fibres did not reach the largest strains of the native capsule.

Hysteresis values for the electrospun fibres were greater than those of the native egg capsule, indicating that the nanofibres lost more energy as heat during their loading and unloading cycle.

There is an important source of error in the mechanical data that should be considered. It is very likely that the cross-sectional areas of the samples were over-estimated since measurements were taken once the samples were hydrated. Each electrospun sample tested was made of a loose network of semi-aligned nano-fibres. The samples were very low mass and density, and it would be generous to assume that they were 10% fibre. Therefore, 90% of the volume of the sample would be the medium, which during mechanical testing was water. The result of this is that the stress values determined in this study are all too low, probably by 1 or 2 orders of magnitude. The actual cross-sectional area of the fibres would need to be measured to give more accurate data. If this assessment of the underestimated stress values is correct, the cross-linked electrospun fibres are closer in their mechanical behaviour to the native protein than it originally appeared.

4.12 *Future directions*

The mechanical integrity of the native whelk egg capsule protein does not arise from any gross structural changes in the ventral pedal gland (Rapoport and Shadwick, 2007). Cross-linking during VPG treatment is the most likely source of the stability that gives the mature capsule its interesting mechanical properties. The fact that the mechanical behaviour develops sequentially gives hope that the mysterious cross-linking step will be identified and effectively mimicked in the future.

Different cross-linking agents could be tested on the electrospun fibres, and cross-linking agents with more specific actions could shed more light on what is occurring in the maturation process. Although the nanofibres are delicate, it may be possible to

mechanically manipulate them in a way that mimics the muscular massage of the VPG to see if that has an effect on their mechanical properties.

Mechanical testing could be attempted on dry samples of electrospun fibres and compared to data from dry capsule testing. Samples could also be subjected to repeated hysteresis loops in order to determine the conditioned behaviour. Pre-conditioned samples could be treated with cross-linking agents, or cross-linking treatments could be carried out while the samples are going through a series of loading and unloading cycles.

In order to more accurately model both the protein and the electrospun fibres, it would be interesting to analyze FTIR spectra collected with the material held at different strains, and with the sample hydrated. This could determine changes in secondary structure as strain is increased or water is introduced. Fibres held at constant strain could also have FTIR spectra collected over time to gather information on the mechanism for stress relaxation.

It would also be interesting to monitor the birefringence of the electrospun protein blend fibres as they are strained, to determine if their behaviour is the same as that of microscopic fibres teased out of the egg capsule. Even the electrospinning solution could be tested for birefringence, and compared to the spun fibres. Since the charge-aligned nanofibres are presumably a more ordered structure than the homogenized solution, we would expect the fibre birefringence to be greater than that of the solution.

The whelk egg capsule is a fascinating material, and little is known about it to date. Its interesting properties deserve more exhaustive study, like that devoted to other structural proteins.

References

Aaron, B.B. and Gosline, J.M. (1980). Optical properties of single elastin fibres indicate random protein conformation, *Nature* **287**, 865-867.

Altman, G.H., Horan, R.L., Lu, H.H., Moreau, J., Martin, I., Richmond, J.C., and Kaplan, D.L. (2002). Silk matrix for tissue engineered anterior cruciate ligaments, *Biomaterials* **23**, 4131-4141.

Aluigi, A., Vineis, C., Varesano, A., Mazzuchetti, G., Ferrero, F., and Tonin, C. (2008). Structure and properties of keratin/PEO blend nanofibres, *European Polymer Journal* **44**, 2465-2475.

Barnes, C.P., Pemble, C.W., Brand, D.D., Simpson, D.G., and Bowlin, G.L. (2007). Cross-linking electrospun type II collagen tissue engineering scaffolds with carbodiimide in ethanol, *Tissue Engineering* **13**, 1593-1605.

Bellingham, C.M., Lillie, M.A., Gosline, J.M., Wright, G.M., Starcher, B.C., Bailey, A.J., Woodhouse, K.A., and Keeley, F.W. (2003). Recombinant human elastin polypeptides self-assemble into biomaterials with elastin-like properties, *Biopolymers* **70**, 445-455.

Bonnier, F., Rubin, S., Debelle, L., Ventéo, L., Pluot, M., Baehrel, B., Manfait, M., and Sockalingum, G.D. (2008). FTIR protein secondary structure analysis of human ascending aortic tissues, *Journal of Biophotonics* **1**, 204-214.

Brusca, R.C. and Brusca, G.J. (2002). *Invertebrates*, 2nd edition. Sinauer Associates Inc. Publishers, Sunderland, MA.

Buttafoco, L., Kolkman, N.G., Engbers-Buijtenhuijs, P., Poot, A.A., Dijkstra, P.J., Vermes, I., and Feijen, J. (2006). Electrospinning of collagen and elastin for tissue engineering applications, *Biomaterials* **27**, 724-734.

Chen, C., Chuanbao, C., Xilan, M., Yin, T., and Hesun, Z. (2006). Preparation of non-woven mats from all-aqueous silk fibroin solution with electrospinning method, *Polymer* **47**, 6322-6327.

Chen, Z., Mo, X., and Qing, F. (2007). Electrospinning of collagen-chitosan complex, *Materials Letters* **61**, 3490-3494.

Didier, D.W. (2009). Using birefringence as a tool to investigate biomechanical properties of an elastic biopolymer protein. MSc thesis, University of British Columbia, Canada.

Fang, D., Chang, C., Hsiao, B.S., and Chu, B. (2006). Development of multi-jet electrospinning technology. In *American Chemical Society Symposium Series 918*:

Polymeric Nanofibres, (ed. D.H. Reneker and H. Fong), pp 91-105. Washington DC: Oxford University Press/American Chemical Society.

Flower, N.E. (1973). The storage and structure of proteins used in the production of egg capsules by the mollusc *Cominella maculosa*, *Journal of Ultrastructure Research* **44**, 134-145.

Flower, N.E., Geddes, A.J., and Rudall, K.M. (1969). Ultrastructure of the fibrous protein from the egg capsules of the whelk *Buccinum undatum*, *Journal of Ultrastructure Research* **26**, 262-273.

Formhals, A. (1934). Process and apparatus for preparing artificial threads (US Patent 1,975,504) US Patent and Trademark Office.

Fudge, D.S., and Gosline, J.M. (2004). Molecular design of the α -keratin composite: insights from a matrix-free model, hagfish slime threads. *Proceedings of the Royal Society of London* **271**, 291-299.

Gandhi, M.R. (2006). Silk protein as a biomaterial for tissue engineering application: theoretical and experimental study. PhD thesis, Drexel University, Philadelphia, USA.

Goldsmith, L.A., Hanigan, H.M., Thorpe, J.M., and Lindberg, K.A. (1978). Nidamental gland precursor of the egg capsule protein of the gastropod mollusc *Busycon carica*, *Comparative Biochemistry and Physiology* **59** (B), 133-138.

Gosline, J.M. (1980). The elastic properties of rubber-like proteins and highly extensible tissues. In *The Mechanical Properties of Biological Materials, 34th Symposium of the Society for Experimental Biology* (ed. J.F.V. Vincent and J.D. Currey), pp 331-357. Cambridge: Cambridge University Press.

Gosline, J.M., Nichols, C., Guerette, P.A., Cheng, A., and Katz, S. (1995). The macromolecular design of spider's silks. In *Biomimetics: Design and Processing of Materials* (ed. M. Sarikaya and I.A. Aksay), pp 237-261. Woodbury, NY: American Institute of Physics.

Gupta, P. (2004). Processing-structure-property studies on submicron fibres produced by electrospinning. PhD Thesis, Virginia Polytechnic Institute and State University.

Hearle, J.W.S. (2000). A critical review of the structural mechanics of wool and hair fibres, *International Journal of Biological Macromolecules* **27**, 123-138.

Hunt, S. (1966). Carbohydrate and amino-acid composition of the egg capsule of the whelk *Buccinum undatum* L. *Nature* **210**, 436-437.

Jeong, S.I., Kim, S.Y., Cho, S.K., Chong, M.S., Kim, K.S., Kim, H., Lee, S.B., and Lee, Y.M. (2007). Tissue-engineered vascular grafts composed of marine collagen and PLGA fibers using pulsatile perfusion bioreactors, *Biomaterials* **28**, 1115-1122.

Katti, D.S., Robinson, K.W., Ko, F.K., and Laurencin, C.T. (2004). Bioresorbable nanofiber-based systems for wound healing and drug delivery: Optimization of fabrication parameters, *Journal of Biomedical Materials Research B – Applied Biomaterials* **70**, 286-296.

Keeley, F.W., Bellingham, C.M., and Woodhouse, K.A. (2002). Elastin as a self-organizing biomaterial: use of recombinantly expressed human elastin polypeptides as a model for investigators of structure and self-assembly of elastin, *Philosophical Transactions of the Royal Society of London B* **357**, 185-189.

Kreplak, L., Doucet, J., Dumas, P., and Briki, F. (2004). New aspects of the α -helix to β -sheet transition in stretched hard α -keratin fibers, *Biophysical Journal* **87**, 640-647.

Li, C., Vepari, C., Jin, H.J., Kim, H.J., and Kaplan, D.L. (2006). Electrospun silk-BMP-2 scaffolds for bone tissue engineering, *Biomaterials* **27**, 3115-3124.

Li, M., Mondrinos, M.J., Gandhi, M.R., Ko, F.K., Weiss, A.S., and Lelkes, P.I. (2005). Electrospun protein fibres as matrices for tissue engineering, *Biomaterials* **26**, 5999-6008.

Matthews, J.A., Wnek, G.E., Simpson, D.G., and Bowlin, G.L. (2002). Electrospinning of collagen nanofibres, *Biomacromolecules* **3**, 232-238.

Min, B.M., Lee, G., Kim, S.H., Nam, Y.S., Lees, T.S., and Park, W.H. (2004). Electrospinning of silk fibroin nanofibres and its effect on the adhesion and spreading of normal human keratinocytes and fibroblasts in vitro, *Biomaterials* **25**, 1289-1297.

Miserez, A., Wasko, S.S., Carpenter, C.F., and Waite, J.H. (2009). Non-entropic and reversible long-range deformation of an encapsulating bioelastomer, *Nature Materials* **8**, 910-916.

Ojeda, J.A. and Chaparro, O.R. (2004). Morphological, gravimetric, and biochemical changes in *Crepidula fecunda* (Gastropoda: Calyptraeidae) egg capsule walls during embryonic development, *Marine Biology* **144**, 263-269.

Pechenik, J.A. (1979). Role of encapsulation in invertebrate life histories. *The American Naturalist* **114**, 859-870.

Petibois, C., Gouspillou, G., Wehbe, K., Delage, J.P., and Déléris, G. (2006). Analysis of type I and IV collagens by FT-IR spectroscopy and imaging for a molecular investigation of skeletal muscle connective tissue, *Analytical and Bioanalytical Chemistry* **386**, 1618-2650.

- Ramakrishna, S., Fujihara, K., Teo, W.E., Lim, T.C., and Ma, Z. (2005). *An Introduction to Electrospinning and Nanofibres*, Danvers, MA: World Scientific Publishing Co. Pte. Ltd.
- Rapoport, H.S. (2003). Biomechanics, biochemistry, and molecular biology of a molluscan scleroprotein elastomer: whelk egg capsules. PhD thesis, University of California, San Diego, USA.
- Rapoport, H.S. and Shadwick, R.E. (2002). Mechanical characterization of an unusual elastic biomaterial from the egg capsules of marine snails (*Busycon* spp.), *Biomacromolecules* **3**, 42-50.
- Rapoport, H.S. and Shadwick, R.E. (2007). Reversibly labile, sclerotization-induced elastic properties in a keratin analog from marine snails: whelk egg capsule biopolymer (WECB), *Journal of Experimental Biology* **210**, 12-26.
- Rawlings, T.A. (1999). Adaptations to physical stresses in the intertidal zone: the egg capsules of neogastropod mollusks, *American Zoologist* **39**, 230-243.
- Reneker, D.H. and Fong, H. (2006). Polymeric nanofibres: introduction. In *American Chemical Society Symposium Series 918: Polymeric Nanofibres*, (ed. D.H. Reneker and H. Fong), pp 1-6. Washington DC: Oxford University Press/American Chemical Society.
- Savage, K.N. and Gosline, J.M. (2008). The effect of proline on the network structure of major ampullate silks as inferred from their mechanical and optical properties, *Journal of Experimental Biology* **211**, 1937-1947.
- Savage, K.N., Guerette, P.A., and Gosline, J.M. (2004). Supercontraction stress in spider webs, *Biomacromolecules* **5**, 675-679.
- Schreuder-Gibson, H.L., and Gibson, P. (2006). Applications of electrospun nanofibres in current and future materials. In *American Chemical Society Symposium Series 918: Polymeric Nanofibres*, (ed. D.H. Reneker and H. Fong), pp 121-136. Washington DC: Oxford University Press/American Chemical Society.
- Spasova, M., Stoilova, O., Manolova, N., Altankov, G., and Rashkov, I. (2007). Preparation of PLLA/PEG nanofibres by electrospinning and potential applications, *Journal of Bioactive and Compatible Polymers* **22**, 62-76.
- Stuart, B., and Ando, D.J. (1997). *Biological Applications of Infrared Spectroscopy*, New York: John Wiley and Sons.
- Sukigara, S., Gandhi, M., Ayutsede, J., Micklus, M., and Ko, F. (2003). Regeneration of *Bombyx mori* silk by electrospinning. Part 2: Process optimization and empirical modeling using response surface methodology, *Polymer* **45**, 3701-3708.

Sukigara, S., Gandhi, M., Ayutsede, J., Micklus, M., and Ko, F. (2004). Regeneration of *Bombyx mori* silk by electrospinning – part 1: processing parameters and geometric properties, *Polymer* **44**, 5721-5727.

Sukigara, S., Gandhi, M., Ayutsede, J., Micklus, M., and Ko, F. (2005). Regeneration of *Bombyx mori* silk by electrospinning. Part 3: characterization of electrospun nonwoven mat, *Polymer* **46**, 1625-1634.

Sullivan, C.H. and Maugel, T.K. (1984). Formation, organization, and composition of the egg capsule of the marine gastropod, *Ilyanassa obsoleta*. *Biological Bulletin* **167**, 378-389.

Taylor, G.I. (1969). Electrically driven jets. *Proceedings of the Royal Society A* **313**, 453-475.

Teo, W.E. and Ramakrishna, S. (2006). A review on electrospinning design and nanofibre assemblies. *Nanotechnology* **17**, R89-R106.

Treloar, L.R.G. (1982). *Introduction to polymer science*. Taylor and Francis Ltd, London.

Van Steensel, M.A.M., Happle, R., and Steijlen, P.M. (2000). Molecular genetics of the hair follicle: the state of the art, *Proceedings of the Society for Experimental Biology and Medicine* **223**, 1-7.

Yamashita, Y., Tanaka, A., and Ko, F. (2007). Characteristics of elastomeric nanofibre membranes produced by electrospinning. *Journal of Textile Engineering* **53**, 137-142.

Yang, Y., Jia, Z., Li, Q., and Guan, Z. (2006). Experimental investigation of the governing parameters in the electrospinning of polyethylene oxide solution. *IEEE Transactions on Dielectrics and Electrical Insulation* **13** (3), 580-585.

Zeleny, J. (1917). Instability of electrified liquid surfaces. *Physical Review, Second Series* **10** (1).